Mazhar Abbas

WhatsApp: 03489895082, Cell: 03489895082

E-mail# mazharabbas0654@gmail.com

Career Objective:

I am sincere with my profession and trying to achieve the highest of my field. I am looking forward to work for a reputable organization that gives employees, opportunities to enhance and utilize their potentials.

Personal information:

- Father name — Liaqat Ali
- Nationality — Pakistani
- CNIC No. — 37105-6049773-9

Degree	Institute/University	Percentage/C.G.P.A
MS Mathematics (2020-2022)	CUI, Attock	3.23/4.0
M.Sc. Mathematics (2017-2019)	CUI, Attock	3.13/4.0
B.Sc. (Maths A, Maths B, Phy) (2015-2017)	University of the Punjab	55%
F.Sc (Pre-Engineering)	BISE, Rawalpindi	64%
S.S.C	BISE, Rawalpindi	82%

Teaching Experience:

4 Years Teaching Experience.

As a Lecturer

- Prepare and delivering regular lectures.
- Guide class discussions, whilst encouraging debates and feedback among students.
- Prepare and mark student assignment, Exams and provide one-on-one feedback on academic performance where necessary.

Thesis Titles:

MS Thesis Title: Thermal Convection in Nanofluids for Peristaltic Flow in a Non-uniform Channel

Courses Studied:

M. Sc	MS
1. Real Analysis	1.Finite Fields
2. Algebra (Group theory, vector spaces)	2.Heat Transfer
3. Complex Analysis and Differential Geometry	3. Hilbert Spaces
4. Topology and Functional Analysis	4. Viscous Fluids
5. Mechanics	5. Advance Graph Theory
6. Fluid mechanics	6. Advance Numericals
6. PDEs	7. Fixed Point Theory
7. Numerical Analysis	8. Numerical Solution of ODEs
8. Operation Research	
9. Special theory of relativity and Analytical dynamics	
10. Mathematical Statistics	

Publications

1. Thermal convection in nanofluids for peristaltic flow in a nonuniform channel

Sharifah E. Alhazmi, Ali Imran, Mazhar Abbas, Muhammad Awais, ,

Scientific Reports **volume 12**, Article number: 12656 (2022) https://www.nature.com/articles/s41598-022-16600-w

2. Electro osmotic flow of nanofluids within a porous symmetric tapered ciliated channel

Ali Imran, Mazhar Abbas, Saeed Ehsan Awan ,Muhammad Shoaib

https://onlinelibrary.wiley.com/doi/10.1002/zamm.202300838

scientific reports

OPEN

Thermal convection in nanofluids for peristaltic flow in a nonuniform channel

Sharifah E. Alhazmi[1]✉, Ali Imran[2]✉, Muhammad Awais[2], Mazhar Abbas[2], Weaam Alhejaili[3], Haneen Hamam[4], Awatif Alhowaity[5] & Asif Waheed[2]

A magneto couple stress nanofluid flow along with double diffusive convection is presented for peristaltic induce flow through symmetric nonuniform channel. A comprehensive mathematical model is scrutinized for couple stress nanofluid magneto nanofluids and corresponding equations of motions are tackled by applying small Reynolds and long wavelength approximation in viewing the scenario of the biological flow. Computational solution is exhibited with the help of graphical illustration for nanoparticle volume fraction, solutal concentration and temperature profiles in MATHEMTICA software. Stream function is also computed numerically by utilizing the analytical expression for nanoparticle volume fraction, solutal concentration and temperature profiles. Whereas pressure gradient profiles are investigated analytically. Impact of various crucial flow parameter on the pressure gradient, pressure rise per wavelength, nanoparticle volume fraction, solutal concentration, temperature and the velocity distribution are exhibited graphically. It has been deduced that temperature profile is significantly rise with Brownian motion, thermophoresis, Dufour effect, also it is revealed that velocity distribution really effected with strong magnetic field and with increasing non-uniformity of the micro channel. The information of current investigation will be instrumental in the development of smart magneto-peristaltic pumps in certain thermal and drug delivery phenomenon.

List of symbols

V, U	Respective velocity component in Y and X directions
b	Wave amplitude
a	Axial distance width
E	Induced electric field
Θ	Volume fraction of nanoparticle
D_B	Brownian diffusion coefficient
D_s	Solutal diffusion parameter
R_m	Magnetic Reynolds number
G	Gravitational acceleration
T	Temperature
p	Pressure
b_0	Half width at inlet
c	Propagation of velocity
C	Solutal concentration
D_{TC}	Dufour diffusively
N_t	Thermophoresis parameter
N_{CT}	Soret parameter

[1]Mathematics Department, Al-Qunfudah University College, Umm Al-Qura University, Mecca, Kingdom of Saudi Arabia. [2]Department of Mathematics, COMSATS University Islamabad, Attock Campus, Kamra Road, Attock 43600, Pakistan. [3]Department of Mathematical Sciences, College of Science, Princess Nourah bint Abdulrahman University, P.O. Box 84428, Riyadh 11671, Saudi Arabia. [4]Mathematics Department, Umm Al-Qura University, Makkah, Kingdom of Saudi Arabia. [5]Department of Mathematics, College of Science and Arts at Alkamil, University of Jeddah, Jeddah, Saudi Arabia. ✉email: sehazmi@uqu.edu.sa; ali.imran@cuiatk.edu.pk

Greek symbols

σ	Electrical conductivity
μ_e	Magnetic permeability
α	Occlusion ratio
β_T	Volumetric thermal expansion
ρ_p	Mass density of nanoparticle
$(\rho c)_f$	Heat capacitance of fluid
γ	Solutal concentration
θ	Dimensionless temperature
μ	Viscosity of fluid
Ω	Nanoparticle volume fraction
λ	Wave length
ρ_{f0}	Fluid density at T_0
β_C	Volumetric expansion
$(\rho c)_p$	Heat capacity of nanoparticle
N_b	Brownian motion parameter
D_T	Thermophoresis diffusion coefficient
N_{TC}	Dufour parameter

The nonlinear flows involving peristalsis phenomenon are achieving new horizons in view of their core applications in the transport processes in the domains of chemical and biomedical science (bile ducts, esophagus, uterine cavity etc.), bio plasma transport etc. Mathematical modelling involving formulation of the peristaltic processes has tremendous applications in engineering and industries. For-instance Ellahi[1] investigated characteristics of heat and mass transport for the peristaltic flow in a non-uniform rectangular duct. Authors have studied and presented several important results regarding the bioheat transfer model due to its applications in thermotherapy and human thermoregulation system. Sreenadh[2] studied the peristaltic flow of conducting nanofluids in a non-symmetric channel with slip effects of velocity, temperature and concentration. Sharma[3] analyzed the electro-osmosis based peristaltic flow of nanofluid. Authors have investigated the double diffusive convection phenomenon. Awais et al.[4] studied the second law properties and endoscopy applications for hydro magnetic peristaltic flow of nanofluid. Slippage phenomenon along with permeable surface on peristaltic flow of hydro magnetic Ree Eyring nanofluid has been studied by Tanveer and Malik[5]. They have investigated the comprehensive study in a curved channel with porous media by utilizing the modified Darcy's law. Riaz et al.[6] analyzed the peristaltic propulsion of Jeffery nanomaterial. They have studied the heat transfer characteristics within duct with dynamic wall and permeable medium. Heat transfer properties of biological nanoliquid flow dynamics through ductus efferentus have been presented by Imran et al.[7]. Hydro magnetic analysis and heat transfer effects through ductus efferentus involving variable viscosity phenomenon has been analyzed by Imran et al.[8]. Thermal and micro rotation process involving Cu-CuO/blood nanoparticles in a microvascular geometry has been analyzed by Tripathi et al.[9]. Blood flow of hydro magnetic non-Newtonian nanomaterial involving heat transfer and slip effect has been analyzed by Aasma et al.[10]. Qureshi et al.[11] analyzed impacts of radially magnetic field axioms in a peristaltic flow with internally generated heat phenomena. Parveen et al.[12] studied thermophysical axioms of chemotactic microorganisms in bio-convective peristaltic flow dynamics of nanoliquid with slipp and Joule heating effects. Some latest studies on the recent development on peristaltic phenomenon are presented in Refs.[7,8,13–21].

Divya et al.[22] presented the biological dynamics of a Casson fluid within a non-uniform channel along with radially applied magnetic field. Analytical investigation for unsteady dynamics of a Rabinowitsch fluid through afore mentioned geometry is revealed for variable liquid properties[23].

Note that with the advent of modern computers, numerical computing (one of the latest technique) to perform highly parallel computing involving difficult navigation and recognition tasks have been utilized by many researcher to tackle the complex problems. The approximate solutions have lost some of their significance since recently developed numerical algorithms are available to tackle the progressively realistic and complex problems. It is due to the fact the a computed numerical result, requiring nominal effort with significant precision is mostly useful for scientist, engineers and applied mathematician who may acquire the core insight of the problem easily. Researcher have employed numerical computing recently in a variety of domains. For-instance Singh et al.[24] computed numerical results of micropolar fluid. Authors have considered the flow situation over a stretching surface with chemical reaction along with melting heat transfer. They have employed the Keller-Box method to compute the results. Pandey[25] experimentally investigated with the aid of numerical simulation thermal and flow properties of a shear-thinning non-Newtonian fluid in a varyingly heated cavity. Awais et al.[26] examined the fluid rheology of bioconvective nanofluid possessing dynamic microorganisms with the help of numerical computations and revealed heat and mass transfer phenomena. Salmi et al.[27] also presented numerical study with heat and mass transfer development in Prandtl fluid magnetohydrodynamic flow using Cattaneo-Christov heat flux theory. Awais et al.[28] analyzed generalized MHD impacts in a Sakiadis flow of polymeric nano liquids. In this communication our objective is to explore further in the regime of biological flow computations via numerical computing. The tendency of numerical computing to deal with the complex nature of biological/peristaltic flow model motivates the authors to investigate the double-diffusive convection process via thermal and concentration properties for the non-uniform biological geometry. Flow dynamics of couple-stress nanomaterial under the application of magnetic field are computed. Mathematical modellings have been performed and dataset is computed and comprehensive studies for emerging physical quantities are performed to examine the outcome

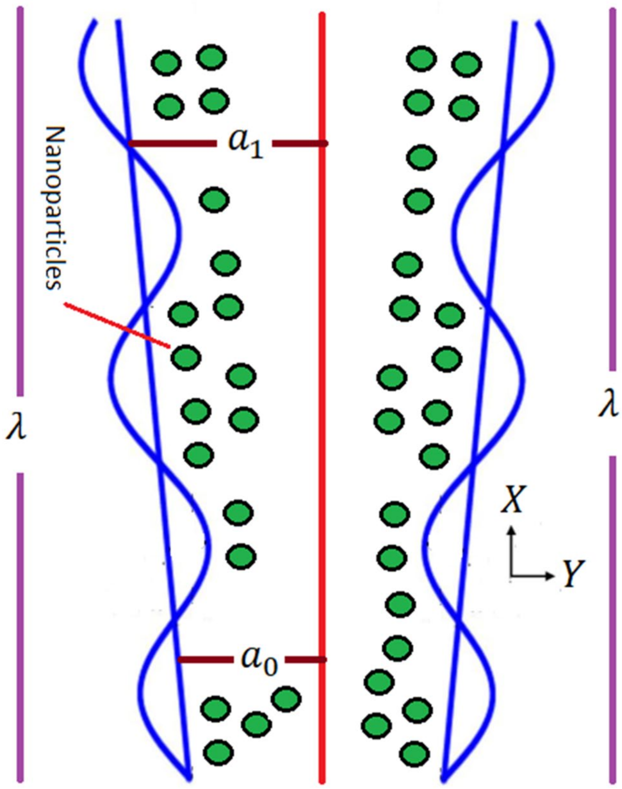

Figure 1. Problem's geometry.

of each term. Tackling such bio-mathematical problems are important to modernize the diagnostic processes of several issues arise in peristaltic phenomenon.

Further physiological impacts are explored for the biological flow of rheological fluid through inclined geometries by[29–33]. Hayat et al.[34] elaborated the effect of thermal radiation along with MHD for the Jeffrey fluid. A mathematical investigation for the peristaltic flow of couple-stress fluid in a transverse non-symmetric channel with bon-isothermal scenario has been reported[35]. One may find related heat transfer analysis for peristaltically induce flow for couple stress fluid[21,36,37].

Mathematical interpretation of physical problem

Let us emphasis on the flow dynamics of electrically conducting couple stress fluid in a nonuniform channel in an incompressible MHD flow. Waves pass alongside the channel walls, causing flow. Assume we have a rectangular coordinate system with the X-axis aligned with wave propagation and the Y-axis parallel to it. The induced magnetic field is led by a continuous magnetic area of strength acting in a transverse direction. The magnetic field in general is defined as (Fig. 1)

$$H^{+}(\tilde{h}_X(X,\ Y,\ t), H_0 + \tilde{h}_Y(X,\ Y,\ t),\ 0).$$

The following is the geometrical description of the physical problem[21–33,33–37]:

$$H(X,t) = b\sin\left(\frac{2\pi}{\lambda_1}(X-ct)\right) + a(X), \tag{1}$$

with $a(X) = a_0 + a_1 X$.

Within equation the parameters λ, a_0, t, a, b, c, represents wavelength, half width at inlet, time, half breadth of channel, wave amplitude, speed of the wave and respectively.

The continuity, momentum, energy, concentration, and nanoparticle volume fraction equations[33,34] are:

$$\left(\frac{\partial U}{\partial X} + \frac{\partial V}{\partial Y}\right) = 0, \tag{2}$$

$$\rho_f\left(\frac{\partial}{\partial t}+U\frac{\partial}{\partial X}+V\frac{\partial}{\partial Y}\right)U=-\frac{\partial P}{\partial X}+\mu\left(\frac{\partial^2 U}{\partial X^2}+\frac{\partial^2 U}{\partial Y^2}\right) -\eta\left(\frac{\partial^4}{\partial X^4}+\frac{\partial^4}{\partial Y^4}+2\frac{\partial^4}{\partial X^2\partial Y^2}\right)U -\frac{\mu_e}{2}\left(\frac{\partial H^{+^2}}{\partial Y}\right)+\mu_e\left(h_X\frac{\partial}{\partial X}+h_Y\frac{\partial}{\partial Y}+H_0\frac{\partial}{\partial Y}\right)h_X +g\{\rho_{f0}(1-\Theta)\{\beta_T(T-T_0)+\beta_C(C-C_0)\} -(\rho-\rho_{f0})(\Theta-\Theta_0)\}. \tag{3}$$

$$\rho_f\left(\frac{\partial}{\partial t}+U\frac{\partial}{\partial X}+V\frac{\partial}{\partial Y}\right)V=-\frac{\partial P}{\partial Y}+\mu\left(\frac{\partial^2 V}{\partial X^2}+\frac{\partial^2 V}{\partial Y^2}\right) -\eta\left(\frac{\partial^4}{\partial X^4}+\frac{\partial^4}{\partial Y^4}+2\frac{\partial^4}{\partial X^2\partial Y^2}\right)V -\frac{\mu_e}{2}(\frac{\partial H^{+^2}}{\partial Y})+\mu_e\left(h_X\frac{\partial h_X}{\partial X}+h_Y\frac{\partial h_X}{\partial Y}+H_0\frac{\partial h_X}{\partial Y}\right) +g\rho_{f0}\{(1-\Theta)\{\beta_T(T-T_0)+\beta_C(C-C_0)\} -(\rho-\rho_{f0})(\Theta-\Theta_0)\}. \tag{4}$$

$$(\rho c)_f\left(U\frac{\partial}{\partial X}+V\frac{\partial}{\partial Y}+\frac{\partial}{\partial t}\right)T=\sigma\left(\frac{\partial^2}{\partial Y^2}+\frac{\partial^2}{\partial X^2}\right)T +(\rho c)_f\left\{D_B\left(\frac{\partial\Theta}{\partial X}\frac{\partial}{\partial X}+\frac{\partial\Theta}{\partial Y}\frac{\partial}{\partial Y}\right)T \left(\frac{D_T}{T_0}\right)\left[\left(\frac{\partial T}{\partial X}\right)^2+\left(\frac{\partial T}{\partial Y}\right)^2\right]\right\}+D_{TC}\left(\frac{\partial^2 C}{\partial X^2}+\frac{\partial^2 C}{\partial Y^2}\right), \tag{5}$$

$$\left(\frac{\partial}{\partial t}+U\frac{\partial}{\partial X}+V\frac{\partial}{\partial Y}\right)C=D_s\left(\frac{\partial^2 C}{\partial X^2}+\frac{\partial^2 C}{\partial Y^2}\right)+D_{TC}\left(\frac{\partial^2 T}{\partial X^2}+\frac{\partial^2 T}{\partial Y^2}\right), \tag{6}$$

$$\left(\frac{\partial}{\partial t}+U\frac{\partial}{\partial X}+V\frac{\partial}{\partial Y}\right)\Theta=\left(\frac{D_T}{T_0}\right)\left(\frac{\partial^2 T}{\partial X^2}+\frac{\partial^2 T}{\partial Y^2}\right)+D_B\left(\frac{\partial^2}{\partial X^2}+\frac{\partial^2}{\partial Y^2}\right)\Theta, \tag{7}$$

In order to further simplified the flow analysis, the following transformations would be used to examine the flow from laboratory frame of situation to wave frame scenario.

$$\widehat{x}=X-ct,\ \widehat{u}=U-c,\ \widehat{y}=Y. \quad \widehat{v}=V, p(\widehat{x},\ \widehat{y})=P(X,Y,t),\ \widehat{C}(\widehat{x},\ \widehat{y})=C(X,Y,t) \quad \widehat{T}(\widehat{x},\ \widehat{y})=T(X,Y,t),\ \widehat{\Theta}(\widehat{x},\ \widehat{y})=\Theta(X,Y,t). \tag{8}$$

Making use of underneath transformations one may have.

$$\widehat{x}=\frac{x}{\lambda_1},\ \overline{y}=\frac{y}{b_0},\ \widehat{v}=\frac{v}{c},\ \widehat{u}=\frac{u}{c},\overline{p}=\frac{b_0^2 p}{\mu c\lambda_1},\ \overline{t}=\frac{ct}{\lambda_1},\ \theta=\frac{\widehat{T}-T_0}{T_1-T_0},\ R_m=\sigma\mu_e b_0 c, \quad \Omega=\frac{\overline{\Theta}-\Theta_0}{\Theta_1-\Theta_0},\ N_{CT}=\frac{D_{CT}(T_1-T_0)}{(C_1-C_0)D_s},\ N_{TC}=\frac{D_{CT}(C_1-C_0)}{\sigma(T_1-T_0)},\ \overline{h}=\frac{h}{b_0},\ \overline{\Phi}=\frac{\Phi}{H_0 b_0}, \quad N_b=\frac{(\rho c)_p D_B(\Theta_1-\Theta_0)}{\sigma},\ N_t=\frac{(\rho c)_p D_T(T_1-T_0)}{T_0\sigma},\ \lambda=\frac{\overline{C}-C_0}{C_1-C_0},\ h_X=\frac{\partial\Phi}{\partial y} \tag{9}$$

Making use of above quantities in Eqs. (2–7) along with long wavelength and low Reynolds numbers we get.

$$-\frac{\partial p}{\partial x}+\frac{\partial^3\psi}{\partial y^3}-\frac{1}{k^2}\frac{\partial^5\psi}{\partial y^5}+G_{rt}\theta+G_{rc}\lambda-G_{rF}\Omega=0 \tag{10}$$

$$\frac{\partial^2\theta}{\partial y^2}+N_{TC}\frac{\partial^2\lambda}{\partial y^2}+N_b\left(\frac{\partial\theta}{\partial y}\frac{\partial\Omega}{\partial y}\right)+N_t\left(\frac{\partial\theta}{\partial y}\right)^2=0, \tag{11}$$

$$\frac{\partial^2\lambda}{\partial y^2}+N_{TC}\frac{\partial^2\theta}{\partial y^2}=0 \tag{12}$$

$$\frac{\partial^2\Omega}{\partial y^2}+\frac{N_t}{N_b}\frac{\partial^2\theta}{\partial y^2}=0, \tag{13}$$

$$\Phi_{yy}=R_m(E-\psi_y), \tag{14}$$

$$\frac{\partial^6\psi}{\partial y^6}-k^2\frac{\partial^4\psi}{\partial y^4}-k^2M^2\left(\frac{\partial^2\psi}{\partial y^2}\right)+k^2(G_{rt}\theta_y+G_{rc}\lambda_y-G_{rF}\Omega_y)=0, \tag{15}$$

The above-mentioned equations are associated with following boundary conditions

$$\theta=0,\ \Omega=0,\ \lambda=0 \text{ on y}=0, \tag{16}$$

$$\theta=1,\ \Omega=1,\ \lambda=1 \text{ on y}=\text{h}, \tag{17}$$

$$\Phi=0 \text{ on y}=h,\ \text{and}\ \ \frac{\partial\Phi}{\partial y}=0 \text{ at y}=0, \tag{18}$$

$$\begin{aligned}&\psi=0,\frac{\partial^2\psi}{\partial y^2}=0,\frac{\partial^4\psi}{\partial y^4}=0 \text{ on y}=0,\\&\psi=F,\frac{\partial\psi}{\partial y}=-1,\frac{\partial^3\psi}{\partial y^3}=0 \text{ on y}=\text{h},\end{aligned} \tag{19}$$

where $\text{h}=1+\text{m}_1x+\alpha\sin(2\pi x)$.

where m_1 non dimensional width of the inlet, α is the non-uniform width[22,23] of the channel.

The expression for current density and axial induced magnetic field is defined as.

$$\text{J}_z=-\frac{\partial \text{h}_X}{\partial y},\ h_x=\frac{\partial\Phi}{\partial y} \tag{20}$$

To explore pressure rise per wavelength we may have.

$$\Delta p=\int_0^1\frac{d\hat{p}}{dx}dx$$

Solution of the problem

Equations (11–13) are tackled numerically in Mathematica, whereas the Eq. (15) after capitalizing exact expressions from Eqs. (21–23) is also solved computationally.

The expression for nanoparticle volume fraction is obtained from Eq. (13) as,

$$\Omega=-\frac{N_t\left(c5(N_{CT}N_{TC}-1)e^{\frac{c2yN_b}{N_{CT}N_{TC}-1}}+c6\right)}{N_b}+c1+c2y, \tag{21}$$

Similarly, the expression for solutal concentration is obtained from Eq. (12) as,

$$\lambda=c3+c4y-\left(-\frac{1}{e^{\frac{c2hN_b}{-1+N_{CT}N_{TC}}}}+\frac{e^{\frac{c2yN_b}{-1+N_{CT}N_{TC}}}}{-1+e^{\frac{c2hN_b}{-1+N_{CT}N_{TC}}}}\right)N_{CT}, \tag{22}$$

By utilizing Eq. (11) the temperature expression is obtained as,

$$\theta=c6+\frac{e^{\frac{c2yN_b}{N_{CT}N_{TC}-1}}c5(-1+N_{CT}N_{TC})}{c2N_b}, \tag{23}$$

The constants c1 through c6 are determined using boundary conditions (16, 17). The following are the values of these constants:

y	Afzal et al.[33]	Current investigation	Absolute error
0	0	0	0
0.2	0.308818	0.308818	1.27191×10^{-9}
0.4	0.530096	0.530096	2.6099×10^{-9}
0.6	0.688648	0.688648	4.13253×10^{-9}
0.8	0.802256	0.802256	4.94762×10^{-9}
1	0.88366	0.88366	6.35472×10^{-9}
1.2	0.941988	0.941988	2.20791×10^{-9}
1.4	0.983782	0.983782	1.74327×10^{-9}
1.6	1.01373	1.01373	1.18178×10^{-9}
1.8	1.03519	1.03519	3.02418×10^{-10}
2	1.05056	1.05056	4.40595×10^{-10}

Table 1. Comparison of temperature profile solution with $x = 1,\ m1 = 0.5,\ \alpha = 0.5,\ N_{TC} = 0.8,\ N_b = 0.1,\ N_t = 0.8,\ N_{CT} = 0.8.$

y	Afzal et al.[33]	Current investigation	Absolut error
0	0	0	0
0.2	−0.00705441	−0.00705441	1.01753×10^{-9}
0.4	0.0559234	0.0559234	2.08791×10^{-9}
0.6	0.169081	0.169081	3.30601×10^{-9}
0.8	0.318195	0.318195	3.95808×10^{-9}
1	0.493072	0.493072	5.08375×10^{-9}
1.2	0.68641	0.68641	1.7663×10^{-9}
1.4	0.892975	0.892975	1.39458×10^{-9}
1.6	1.10902	1.10902	9.45387×10^{-10}
1.8	1.33185	1.33185	2.4189×10^{-10}
2	1.55955	1.55955	3.52426×10^{-10}

Table 2. Comparison of concentration profile solution with $x = 1,\ m1 = 0.5,\ \alpha = 0.5,\ N_{TC} = 0.8,\ N_b = 0.1,\ N_t = 0.8,\ N_{CT} = 0.8.$

$$
\begin{aligned}
&c1 = 0,\ c2 = -\frac{-N_b - N_t}{hN_b},\\
&c3 = 0,\ c4 = -\frac{-1 - N_{CT}}{h},\\
&c5 = \frac{c2N_b}{\left(-1 + e^{\frac{c2hN_b}{-1+N_{CT}N_{TC}}}\right)(-1 + N_{CT}N_{TC})},\\
&c6 = -\frac{1}{-1 + e^{\frac{c2hN_b}{-1+N_{CT}N_{TC}}}},
\end{aligned}
$$

Graphical observations

A magneto couple stress nanofluid flow involving double diffusive convective process has been investigated for peristaltic induced biological problem through non uniform channel. A comprehensive mathematical model is examined for couple stress nanofluid magneto nanofluids. A comparative analysis of current investigation with Afzal et al.[33] are made in Tables 1, 2 and 3. It is evident from Tables 1, 2 and 3 very small absolute error for temperature, concentration and nanoparticle fraction which validate current study. Computations explored with the help of graphical illustration for several biophysical quantities are portrayed in Figs. 2, 3, 4, 5, 6, 7, 8, 9, 10, 11, 12, 13, 14, 15, 16, 17, 18, 19, 20, 21, 22, 23, 24, 25, 26, 27, 28 and 29 for $G_{rF} = 1.5,\ G_{rc} = 1.5,\ G_{rt} = 1.5,\ \alpha = 0.3,\ k = 1.4$. The impacts of several important variables on the nanoparticle fractions, pressure gradient, pressure rise per wavelength, current density distribution, temperature profiles, solutal concentration, axial induced magnetic field and stream function profiles are displayed in graphical and tabular form. Figures 2 and 3 elucidate the influence of non-uniformity parameter $m1$ and thermophoresis parameter N_t on pressure gradient dp/dx. It is revealed from Fig. 2 that an incremental increase in non-uniformity parameter $m1$, the pressure gradient diminishes

y	Afzal et al.[33]	Current investigation	Absolute error
0	0	0	0
0.2	− 1.27054	− 1.27054	1.01753×10^{-8}
0.4	− 1.84077	− 1.84077	2.08792×10^{-8}
0.6	− 1.90919	− 1.90919	3.30603×10^{-8}
0.8	− 1.61805	− 1.61805	3.9581×10^{-8}
1	− 1.06928	− 1.06928	5.08377×10^{-8}
1.2	− 0.335902	− 0.335902	1.76632×10^{-8}
1.4	0.529746	0.529746	1.39461×10^{-8}
1.6	1.49017	1.49017	9.45423×10^{-9}
1.8	2.51851	2.51851	2.41931×10^{-9}
2	3.59551	3.59551	3.52471×10^{-9}

Table 3. Comparison of nanoparticle volume fraction profile solution with $x = 1,\ m1 = 0.5,\ \alpha = 0.5,\ N_{TC} = 0.8,\ N_b = 0.1,\ N_t = 0.8,\ N_{CT} = 0.8.$

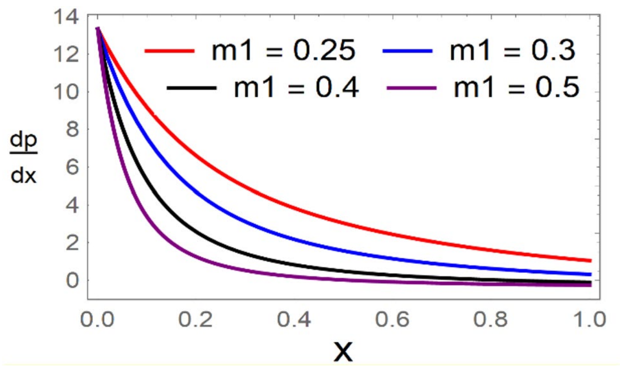

Figure 2. $\frac{dp}{dx}$ profile for m1.

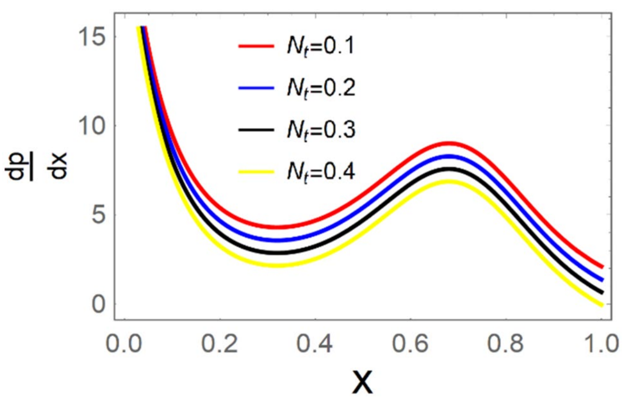

Figure 3. $\frac{dp}{dx}$ profile for N_t.

asymptotically. From physical point of view, it is natural phenomenon since the channel width is enhanced naturally pressure profile will decrease. From Fig. 3, we observed that as the value of thermophoresis parameter N_t enhances, reduction in the pressure gradient is observed. Physically thermophoresis phenomenon results into higher molecular movement which results into a decay in pressure gradient. Figures 4 and 5 exhibit the impacts of non-uniformity parameter *m1* and thermophoresis parameter N_t on the pumping mechanism. It is observed that pumping phenomenon is greatly influenced by these parameters, pressurize profile is depreciated in region $y \in [-2, 1]$ and is surges in $y \in [-1, 4]$ as non-uniformity parameter *m1* is enhanced. Further, it is reported that pressure rise is compactly surges as thermophoresis parameter N_t is strengthened. Figures 6 and 7 show the effects

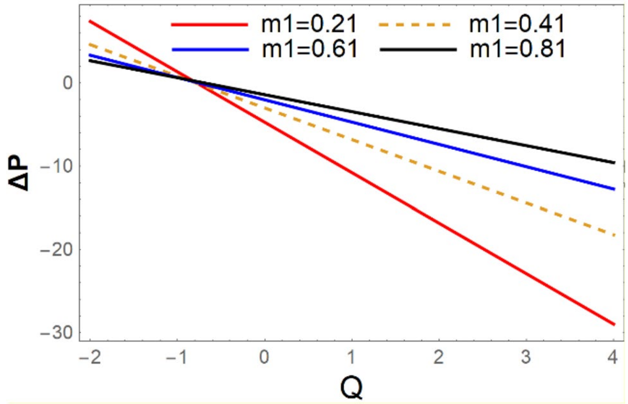

Figure 4. Δp impact for varying m1.

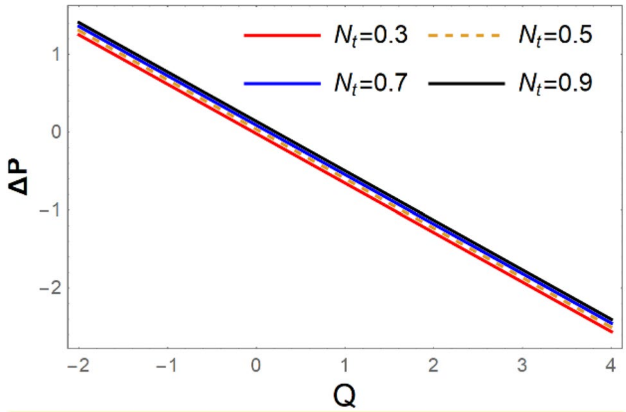

Figure 5. Δp impact for varying profile for N_t.

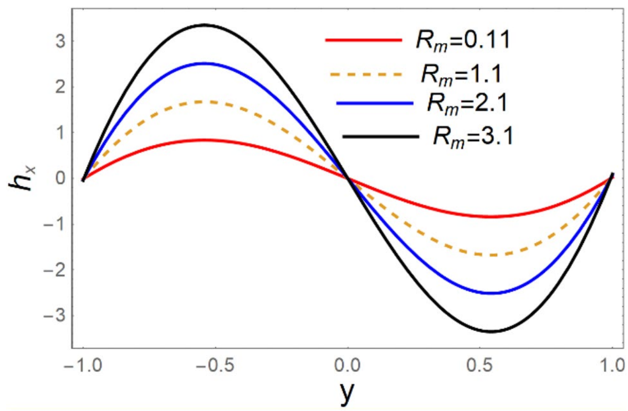

Figure 6. h_x variations for R_m.

of magnetic Reynolds number R_m and Hartmann number M on the axial induced magnetic field h_x. It is quite evident from Fig. 6 that axial induced magnetic field rises in one region $y \in [-1, 0]$ and is repressed in other region $y \in [0, 1].[0, 1]\cdot$ It is due to the fact that magnetic Reynolds number is the ratio of induction and diffusion, it provides a guess of the relative impacts of induction due to magnetic field due to the dynamics of a conducting medium. Figure 7 shows opposite trends for positive values of magnetic field M. Since Hartmann number provides an estimate of the relative significance of drag forces which are generated from magnetic induction and viscous forces during the flow. It may be deduced that axial induced magnetic field distribution is declined initially and then turn around is seen. In order to observe the influences of magnetic Reynolds number R_m and

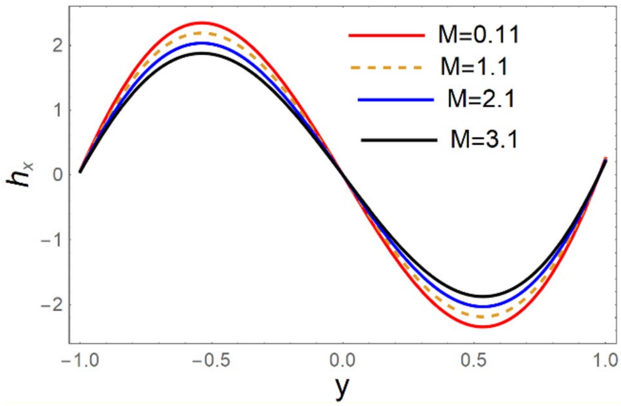

Figure 7. h_x variations for M.

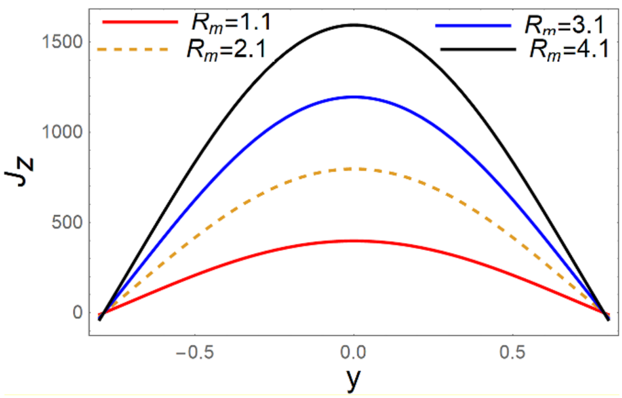

Figure 8. J_z variations for R_m.

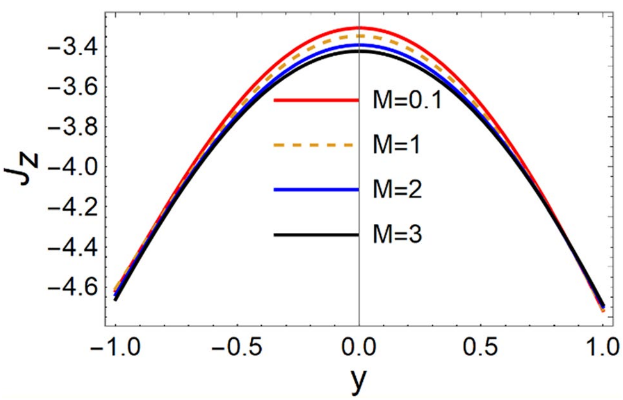

Figure 9. J_z variations for M.

Hartmann number M on the current density J_Z, we have prepared Figs. 8 and 9. Current density is referred as charge per unit time that flows within some specified region. It is quite evident from the Fig. 8 that the magnetic Reynolds number reinforce current density distribution. Further, as narrated above the magnetic number retard the flow, in the similar manner a declined in the current density distribution is observed as magnetic field is become stronger (Fig. 9). Figures 10, 11, 12 and 13 have been prepared in order to investigate the phenomenon of Brownian motion N_b, thermophoresis parameter N_t, Soret parameter N_{CT} and Dufour parameter N_{TC} on the temperature profile θ. It is noticed that temperature profile enhances with an incremental change in Brownian motion N_b, thermophoresis parameter N_t, Soret parameter N_{CT} and Dufour parameter N_{TC}. The qualitative

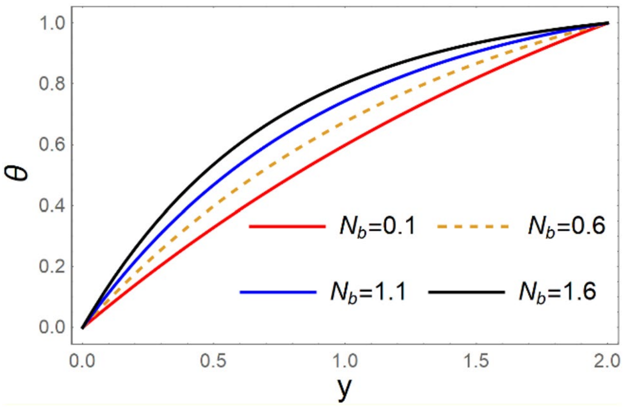

Figure 10. θ variations for N_b.

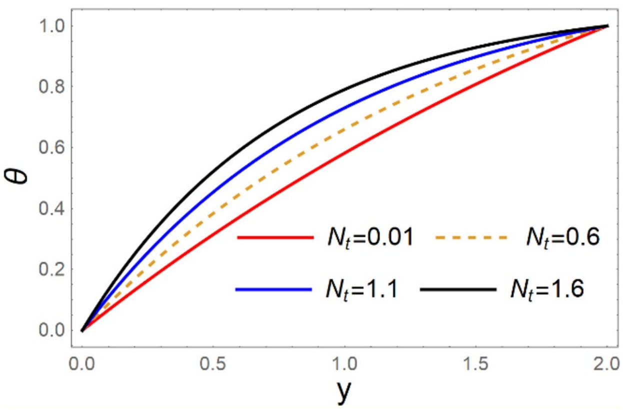

Figure 11. θ variations for N_t.

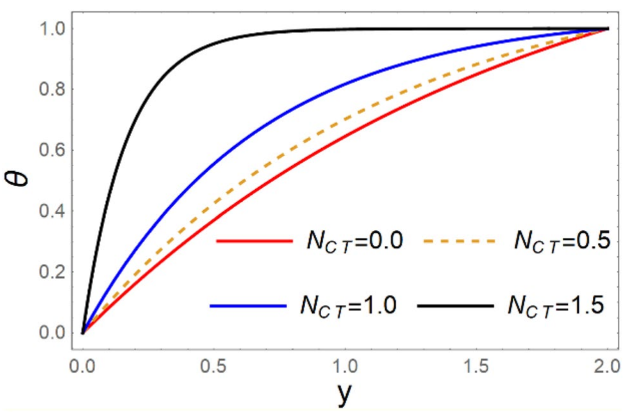

Figure 12. θ variations for N_{CT}.

behavior of Brownian motion N_b, thermophoresis parameter N_t, Soret parameter N_{CT} and Dufour parameter N_{TC} on the temperature profile θ is similar. The effects of Brownian motion N_b, thermophoresis parameter N_t, Soret parameter N_{CT} and Dufour parameter N_{TC} on the solutal concentration profile λ are portrayed in Figs. 14, 15, 16 and 17. We observed that the solutal concentration profile increases with an increase in N_b, N_t, N_{CT} and N_{TC}. Figures 18, 19, 20 and 21 depict the effect of Brownian motion N_b, thermophoresis parameter N_t, Soret parameter N_{CT} and Dufour parameter N_{TC} on nanoparticle fraction Ω. From Fig. 18, it is noted that as the value of N_b increases, the magnitude of nanoparticle fraction Ω increases in magnitude whereas opposite trend is noted for N_t, N_{CT} and N_{TC}. It is also observed maximum variation in nanoparticle fraction Ω is noted near the lower part of

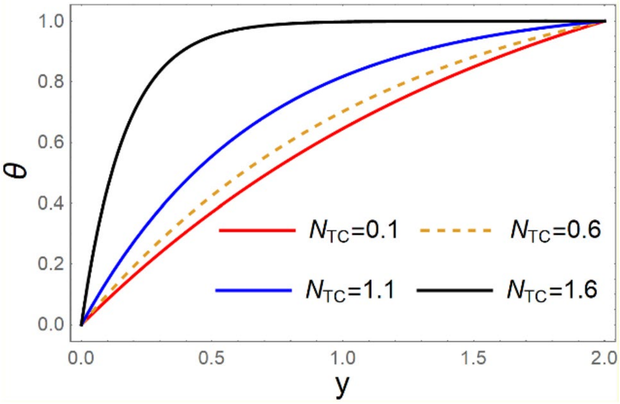

Figure 13. θ variations for N_{TC}.

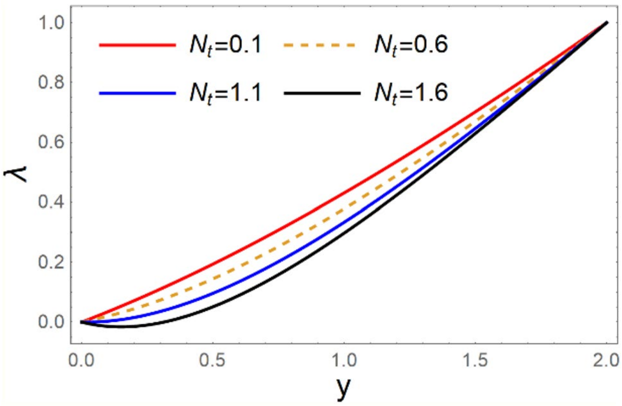

Figure 14. λ profile for N_b.

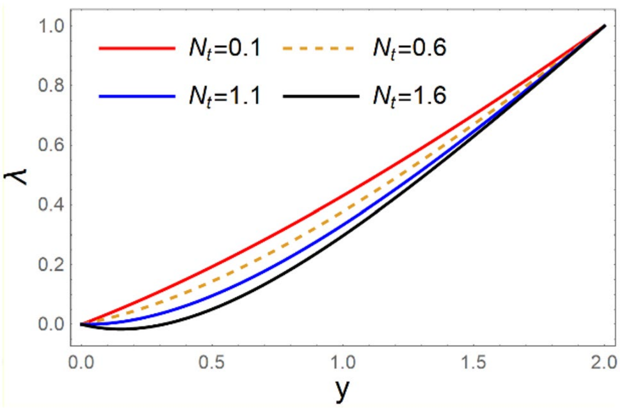

Figure 15. λ profile for N_t.

the channel. Trapping phenomenon play a predominant role in all physiological and its significance is explored in Figs. 22, 23, 24, 25, 26 and 27. It has been experienced that the shape of the trapped bolus is significantly reduced with rising values of K. Furthermore, it is quite obvious from Figs. 24, 25, 26 and 27 that size of trapped bolus is enhanced by increasing the values of Hartmann number M and strengthening the non-uniformity parameter m1. A statistical analysis of temperature and concentration profile as function of thermophoresis N_t is presented in Figs. 28 and 29, it is noticed that temperature profile is lifted with N_t and reverse phenomenon is seen for concentration profile.

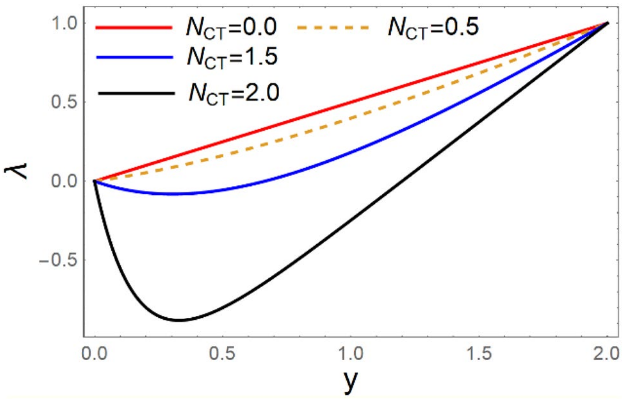

Figure 16. λ variations for N_{CT}.

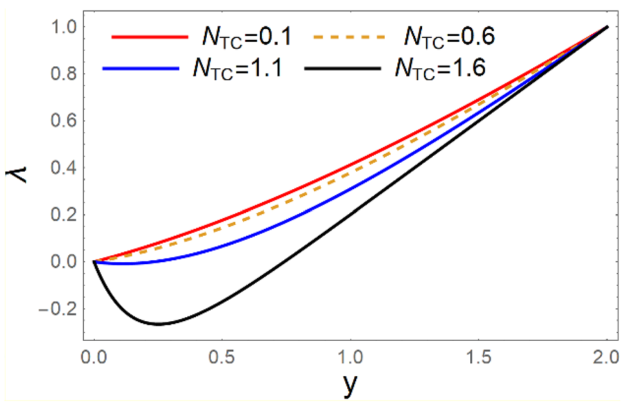

Figure 17. λ variations for N_{TC}.

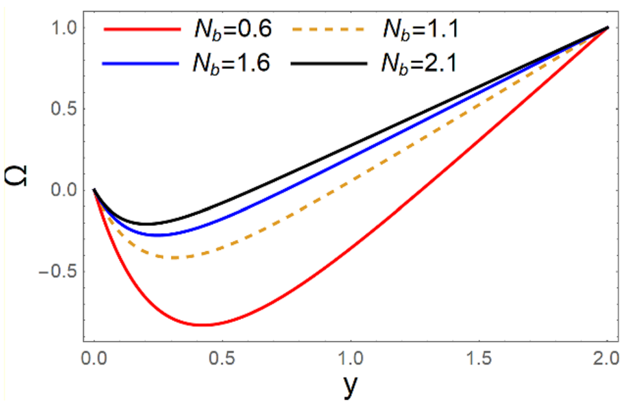

Figure 18. Ω variations for N_b.

Conclusion

A mathematical model has been presented for couple stress magneto nanofluids and corresponding equations of motions are handled by applying low Reynolds and long wavelength approximation in viewing the scenario of the physical flow. Computational solution has been explored for nanoparticle volume fraction, solutal concentration and temperature profiles in MATHEMTICA software. The crux of the current study may be interpreted as:

- The pressure gradient decreases by enhancing the values of thermophoresis and non-uniformity parameter.

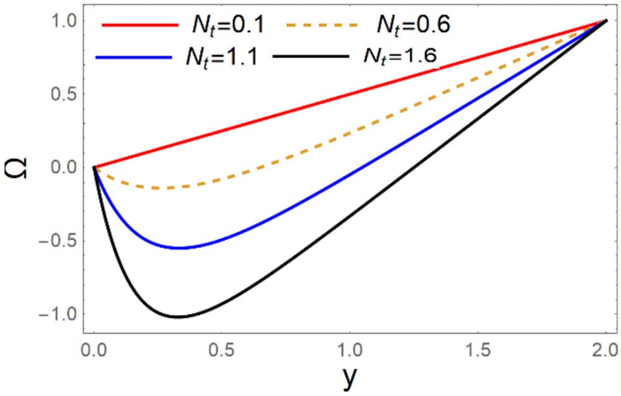

Figure 19. Ω variations for N_t.

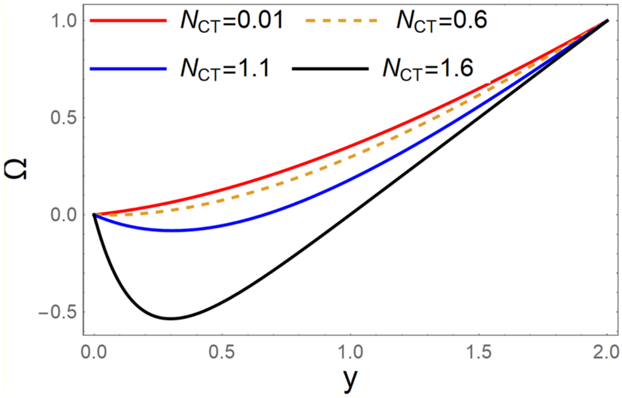

Figure 20. Ω profile for N_{CT}.

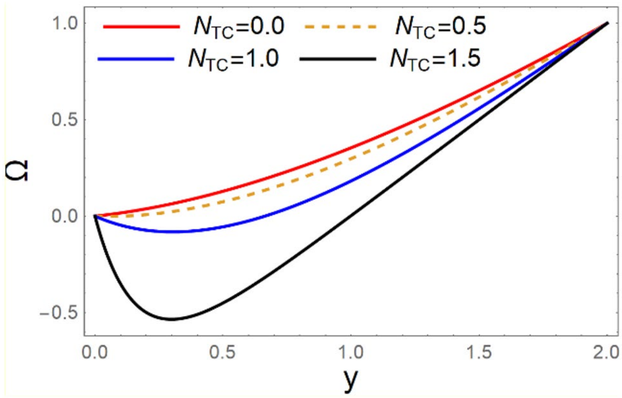

Figure 21. Ω profile for N_{TC}.

- Pressure rise shows increasing behavior by strengthening the values of thermophoresis and non-uniformity parameter.

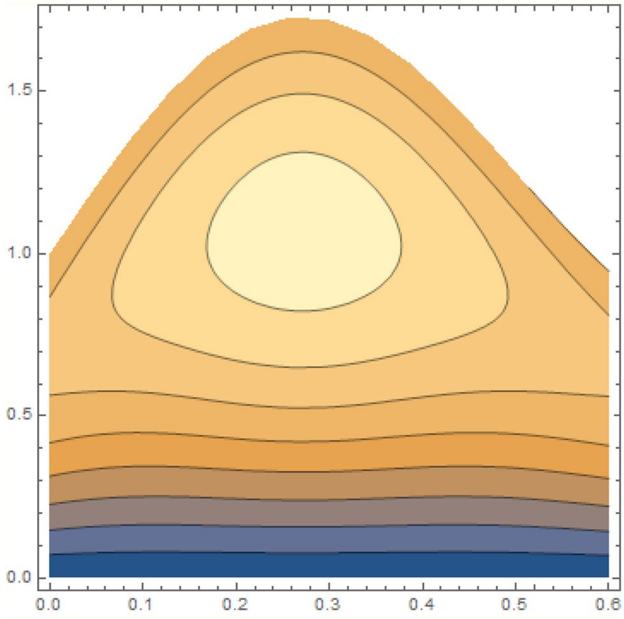

Figure 22. Streamlines of K = 2.5.

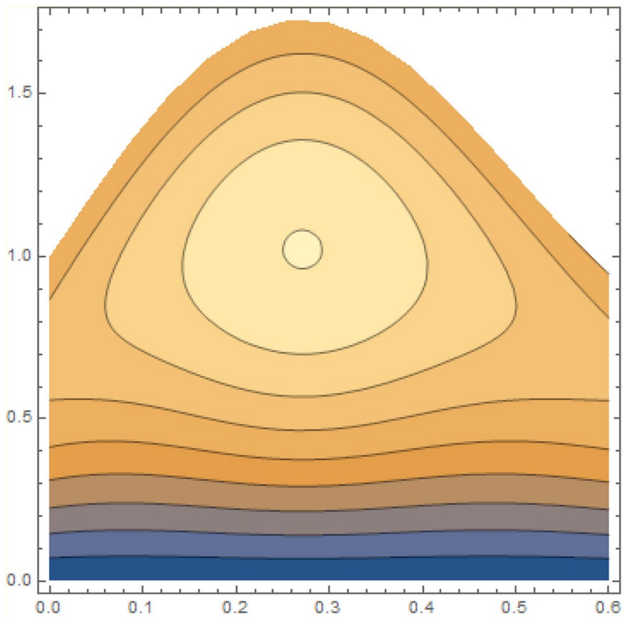

Figure 23. Streamlines of K = 3.5.

- Current density distribution is becoming strong as the magnetic Reynolds number grows and possesses parabolic profile.
- Temperature profiles is lifted with Soret, Brownian motion, thermophoresis diffusion parameter show opposite behavior for concentration profile.
- The Brownian motion parameter shows inverse relation with nanoparticle fraction Ω.
- The trapping bolus is enhanced with strengthening magnetic field and nonuniformity.

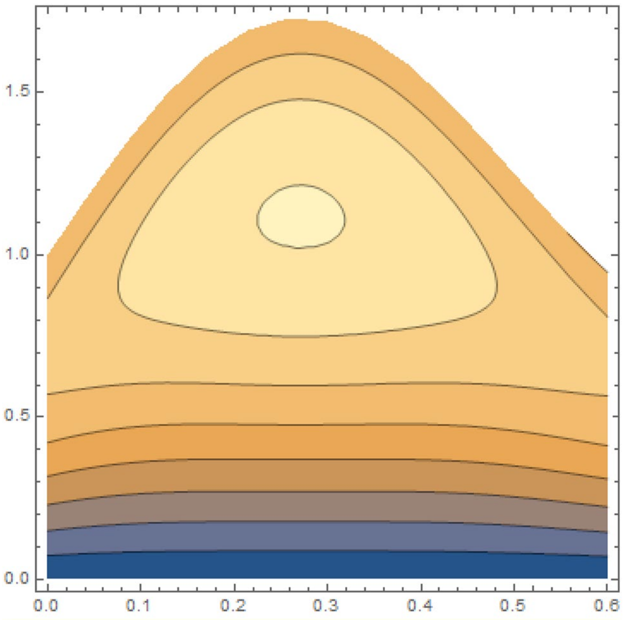

Figure 24. Streamlines of M = 2.0.

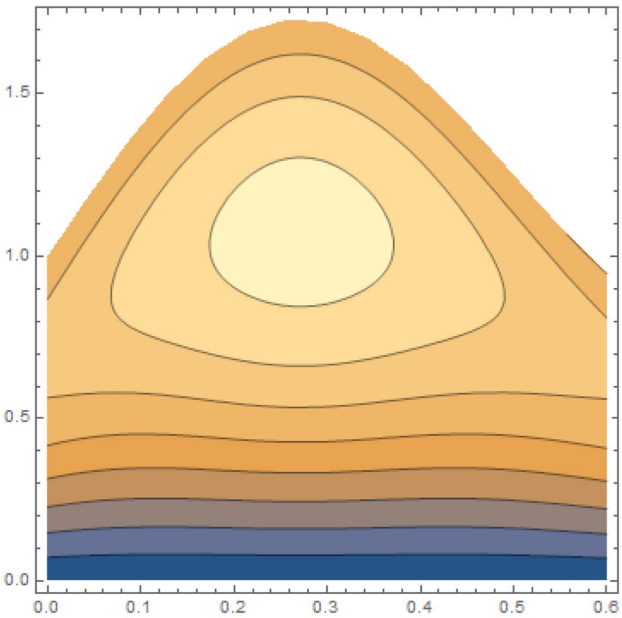

Figure 25. Streamlines of M = 2.2.

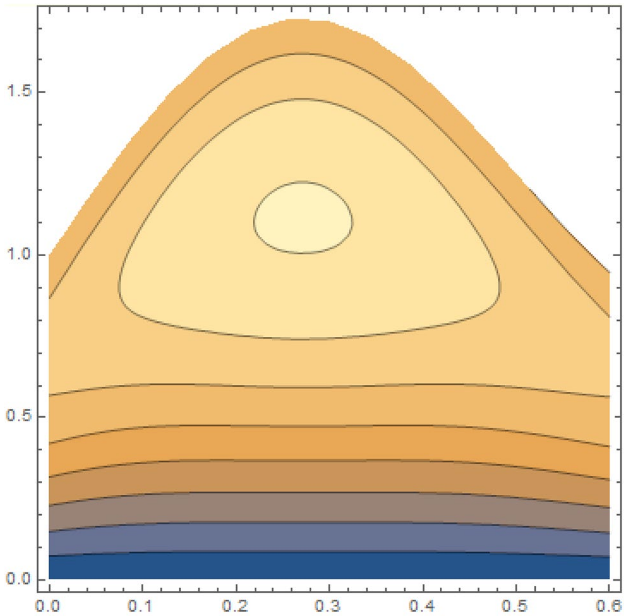

Figure 26. Streamlines of m1 = 0.5.

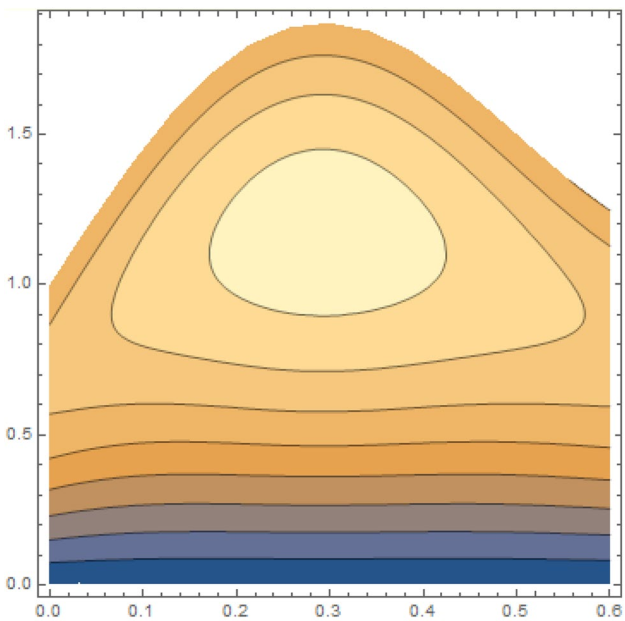

Figure 27. Streamlines of m1 = 1.0.

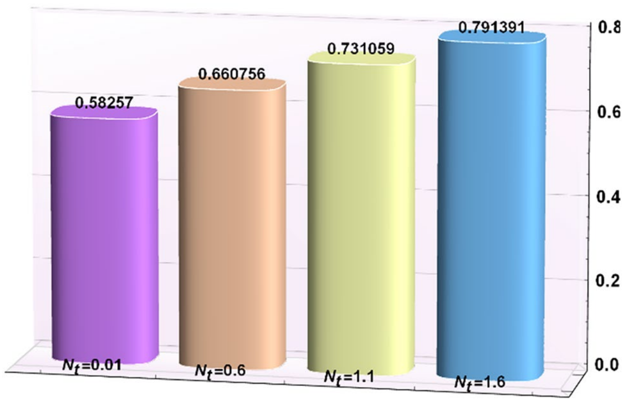

Figure 28. Temperature as function of N_t.

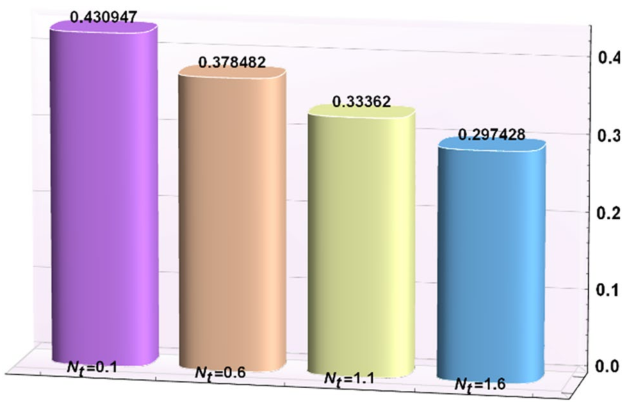

Figure 29. Concentration as function of N_t.

Data availability

All the data is provided within the manuscript.

Received: 24 March 2022; Accepted: 12 July 2022
Published online: 25 July 2022

References

1. Ellahi, R., Bhatti, M. M. & Vafai, K. Effects of heat and mass transfer on peristaltic flow in a non-uniform rectangular duct. *Int. J. Heat Mass Transf.* **71**, 706–719 (2014).
2. Awais, M., Bukhari, U., Ali, A. & Yasmin, H. Convective and peristaltic viscous fluid flow with variable viscosity. *J. Eng. Thermophys.* **26**(1), 69–78 (2017).
3. Sharma, A., Tripathi, D., Sharma, R. K. & Tiwari, A. K. Analysis of double diffusive convection in electroosmosis regulated peristaltic transport of nanofluids. *Physica A* **535**, 122148 (2019).
4. Awais, M., Shoaib, M., Raja, M. A. Z., Arif, S., Malik, M. Y. & Nisar, K. S. Numerical treatment for the second law analysis in hydromagnetic peristaltic nanomaterial rheology: endoscopy applications (2021).
5. Tanveer, A. & Malik, M. Y. Slip and porosity effects on peristalsis of MHD Ree-Eyring nanofluid in curved geometry. *Ain Shams Eng. J.* **12**(1), 955–968 (2021).
6. Riaz, A., Zeeshan, A., Bhatti, M. M. & Ellahi, R. Peristaltic propulsion of Jeffrey nano-liquid and heat transfer through a symmetrical duct with moving walls in a porous medium. *Physica A* **545**, 123788 (2020).
7. Imran, A., Akhtar, R., Zhiyu, Z., Shoaib, M. & Raja, M. A. Z. Heat transfer analysis of biological nanofluid flow through ductus efferentes. *AIP Adv.* **10**(3), 035029 (2020).
8. Imran, A., Akhtar, R., Zhiyu, Z., Shoaib, M. & Raja, M. A. Z. Analysis of MHD and heat transfer effects with variable viscosity through ductus efferentes. *AIP Adv.* **9**(8), 085320 (2019).
9. Tripathi, D., Prakash, J., Tiwari, A. K. & Ellahi, R. Thermal, microrotation, electromagnetic field and nanoparticle shape effects on Cu-CuO/blood flow in microvascular vesselsMicrovasc. *Res.* **132**, 104065 (2020).
10. Elelamy, A. F., Elgazery, N. S. & Ellahi, R. Blood flow of MHD non-Newtonian nanofluid with heat transfer and slip effects: application of bacterial growth in heart valve Int. *J. Numer. Methods Heat Fluid Flow* **30**, 4883–4908 (2020).
11. Qureshi, I. H. *et al.* Influence of radially magnetic field properties in a peristaltic flow with internal heat generation: numerical treatment. *Case Stud. Therm. Eng.* **26**, 101019 (2021).
12. Parveen, N. *et al.* Thermophysical properties of chemotactic microorganisms in bio-convective peristaltic rheology of nano-liquid with slippage, Joule heating and viscous dissipation. *Case Stud. Therm. Eng.* **27**, 101285 (2021).

13. Khan, W. U. *et al.* A novel mathematical modeling with solution for movement of fluid through ciliary caused metachronal waves in a channel. *Sci. Rep.* **11**(1), 1–12 (2021).
14. Zhang, L., Arain, M. B., Bhatti, M. M., Zeeshan, A. & Hal-Sulami, H. Effects of magnetic Reynolds number on swimming of gyrotactic microorganisms between rotating circular plates filled with nanofluids. *Appl. Math. Mech.* **41**, 637–654 (2020).
15. Saqib, M., Ali, F., Khan, I., Sheikh, N. A. & Shafie, S. B. Convection in ethylene glycol-based molybdenum disulfide nanofluid. *J. Therm. Anal. Calorim.* **135**, 523–532 (2019).
16. Choi, S., Singer, D. & Wang, H. Developments and applications of non-Newtonian flows. *ASME Fed.* **66**, 99–105 (1995).
17. Ellahi, R., Raza, M., Vafai, K. & Weinberg, S. L. Series solutions of non- Newtonian nanofluids with Reynolds' model and Vogel's model by means of the homotopy analysis method. *Math. Comput. Model.* **55**, 1876–1891 (2012).
18. Nadeem, S., Riaz, A., Ellahi, R. & Akbar, N. S. Mathematical model for the peristaltic flow of Jeffrey fluid with nanoparticles phenomenon through a rectangular duct. *Appl. Nanosci.* **4**, 613–624 (2014).
19. Akram, S. Nanofluid effects on peristaltic transport of a fourth grade fluid in the occurrence of inclined magnetic field. *Sci. Iran.* **23**, 1502–1516 (2016).
20. Imran, A. *et al.* Investigation of electroosmosis flow of copper nanoparticles with heat transfer due to metachronal rhythm. *Therm. Sci.* **25**(Spec. issue 2), 193–198 (2021).
21. Yasmin, H., Iqbal, N. & Hussain, A. Convective heat/mass transfer analysis on Johnson-Segalman fluid in a symmetric curved channel with peristalsis: engineering applications. *Symmetry* **12**(9), 1475 (2020).
22. Divya, B. B., Manjunatha, G., Rajashekhar, C., Vaidya, H. & Prasad, K. V. Analysis of temperature dependent properties of a peristaltic MHD flow in a non-uniform channel: a Casson fluid model. *Ain Shams Eng. J.* **12**(2), 2181–2191 (2021).
23. Rajashekhar, C. *et al.* Unsteady flow of Rabinowitsch fluid peristaltic transport in a non-uniform channel with temperature-dependent properties. *Alex. Eng. J.* **59**(6), 4745–4758 (2020).
24. Singh, K., Pandey, A. K. & Kumar, M. Numerical solution of micropolar fluid flow via stretchable surface with chemical reaction and melting heat transfer using Keller-Box method. *Propuls. Power Res.* **10**(2), 194–207 (2021).
25. Pandey, S., Yoon, S. Y., Balachandar, S. & Ha, M. Y. Experimental and numerical investigations of thermal and flow characteristics of a shear-thinning non-Newtonian fluid in a differentially heated cavity. *Int. J. Heat Mass Transf.* **187**, 122570 (2022).
26. Awais, M. *et al.* Effects of variable transport properties on heat and mass transfer in MHD bioconvective nanofluid rheology with gyrotactic microorganisms: numerical approach. *Coatings* **11**(2), 231 (2021).
27. Salmi, A. *et al.* Numerical study of heat and mass transfer enhancement in Prandtl fluid MHD flow using Cattaneo-Christov heat flux theory. *Case Stud. Therm. Eng.* **33**, 101949 (2022).
28. Awais, M., Malik, M. Y. & Awan, S. E. Generalized magnetic effects in a Sakiadis flow of polymeric nano-liquids: analytic and numerical solutions. *J. Mol. Liq.* **241**, 570–576 (2017).
29. Vaidya, H. *et al.* Peristaltic flow of non-Newtonian fluid through an inclined complaint nonlinear tube: application to chyme transport in the gastrointestinal tract. *Eur. Phys. J. Plus* **135**(11), 1–15 (2020).
30. Rajashekhar, C. *et al.* Analysis of peristaltic flow of Rabinowitsch fluid in a non-uniform channel: analytical approach. *Lat. Am. Appl. Res.* **50**(3), 151–158 (2020).
31. Manjunatha, G., Rajashekhar, C., Vaidya, H., Prasad, K. V. & Makinde, O. D. Effects wall properties on peristaltic transport of rabinowitsch fluid through an inclined non-uniform slippery tube. in *Defect and Diffusion Forum*, Vol. 392, 138–157. (Trans Tech Publications Ltd., 2019).
32. Vaidya, H. *et al.* Analysis of entropy generation and biomechanical investigation of MHD Jeffery fluid through a vertical non-uniform channel. *Case Studies in Thermal Engineering* **28**, 101538 (2021).
33. Afzal, Q., Akram, S., Ellahi, R., Sait, S. M. & Chaudhry, F. Thermal and concentration convection in nanofluids for peristaltic flow of magneto couple stress fluid in a nonuniform channel. *J. Therm. Anal. Calorim.* **144**(6), 2203–2218 (2021).
34. Hayat, T., Bibi, A., Yasmin, H. & Alsaadi, F. E. Magnetic field and thermal radiation effects in peristaltic flow with heat and mass convection. *J. Therm. Sci. Eng. Appl.* https://doi.org/10.1115/1.4040282 (2018).
35. Hayat, T., Iqbal, M., Yasmin, H., Alsaadi, F. E. & Gao, H. Simultaneous effects of Hall and convective conditions on peristaltic flow of couple-stress fluid in an inclined asymmetric channel. *Pramana* **85**(1), 125–148 (2015).
36. Hayat, T., Tanveer, A., Yasmin, H. & Alsaadi, F. Simultaneous effects of Hall current and thermal deposition in peristaltic transport of Eyring-Powell fluid. *Int. J. Biomath.* **8**(02), 1550024 (2015).
37. Hayat, T., Yasmin, H. & Alsaedi, A. Exact solution for peristaltic flow of a couple stress fluid in an asymmetric channel under convective conditions. *Heat Transf. Res.* **47**(4), 327–342 (2016).

Acknowledgements

This research was funded by Princess Nourah bint Abdulrahman University Researchers Supporting Project number (PNURSP2022R229), Princess Nourah bint Abdulrahman University, Riyadh, Saudi Arabia. The authors also would like to thank the Deanship of Scientific Research at Umm Al-Qura University for supporting this work by Grant Code: (22UQU4282396DSR011).

Author contributions

S. E. and W. A. done overall supervision of the work. A.I., M.A. and M.A. modelled, carried out necessary investigation and analyzed the overall problem. W.A., H.H., A.W. analyzed the numerical data and A.A. concluded the problem.

Competing interests

The authors declare no competing interests.

Additional information

Correspondence and requests for materials should be addressed to S.E.A. or A.I.

Reprints and permissions information is available at www.nature.com/reprints.

Publisher's note Springer Nature remains neutral with regard to jurisdictional claims in published maps and institutional affiliations.

Received: 14 October 2023 | Revised: 17 April 2024 | Accepted: 1 July 2024

DOI: 10.1002/zamm.202300838

ORIGINAL PAPER

Electro osmotic flow of nanofluids within a porous symmetric tapered ciliated channel

Ali Imran[1] | Mazhar Abbas[1] | Saeed Ehsan Awan[2] | Muhammad Shoaib[3] | Muhammad Asif Zahoor Raja[4]

[1]Department of Mathematics, COMSATS University Islamabad, Attock Campus, Attock, Pakistan

[2]Department of Electrical and Computer Engineering, COMSATS University Islamabad, Attock Campus, Attock, Pakistan

[3]Yuan Ze University, AI center, Taoyuan, Taiwan

[4]Future Technology Research center, National Yunlin University of Science and Technology, Douliou, Yunlin, Taiwan

Correspondence
Saeed Ehsan Awan, Department of Electrical and Computer Engineering, COMSATS University Islamabad, Attock Campus, Kamra road Attock, Pakistan.
Email: saeed.ehsan@cuiatk.edu.pk

In this investigation, a comprehensive study has been made to reveal electro osmosis flow through a tapered ciliated symmetric porous channel. The flow is initiated due to metachronal dynamics of cilia. Axial electric field is deployed and thermal radiation phenomenon is scrutinised by applying convective conditions. The equations tackling the flow are non dimensionalized and simplified by capitalizing the low Reynolds number and long wave length approximations. Analytical solution is presented for well reputed Poissson equation and the axial velocity. Whereas, traverse velocity, temperature and nanofluids concentration profiles are examined numerically in MATHEMATICA. Variation of emerging crucial parameters on the velocity profile, temperature and concentration profiles, pressure gradient, pressure rise per wavelength, and on the velocity distribution inside the micro ciliated are exhibited with the aid of graphical deliberations. It worth to mention in this work that in case of tapered channel transverse velocity also has significant contribution in the flow, which is observed trivial in symmetric and non-symmetric channel flows. Temperature of the nanofluid in the ciliated tapered channel is raised with permeability and thermal radiations phenomena and can be controlled with Helmholtz Smoluchowski velocity, and electroosmotic parameter. Pumping phenomena is affected with increase in Helmholtz Smoluchowski velocity and permeability. Reported investigation cover a informative insight about biological fluid system, may be beneficial for the understanding the flow through ductus efferentes of human reproductive tract since it assumed that cilia are responsible for the transport of sperm from rete testis to the epididymis, also have worth in cilia designed bio-sensors and in certain drug delivery systems.

1 | INTRODUCTION

A cilium is a projection from the surface of free cells that looks like a hair. It has been observed in practically every species. Cilia are divided into two categories: motile and non-motile. The significance of motile cilia intend to be highlighted. They are involved in a variety of main phenomena as a result of their motility, all of which are physiologically significant [1]. Rivera [2] has supplied a number of valuable general information and relative data on the cilia of the gills of a variety of species, which can be summarised as follows: (a) In some random tissues, all cilia beat at the same pace. (b) Lashings of cilia on neighbouring cells are meticulously observed. (c) A series of metachronal rhythms. A metachronal rhythm controls the lashing of cilia from one row to the next. Any substance that lives on the premises of cilia persists to travel in a fixed direction. Since the ciliary rhythm adds a constant water passage to the outer part of the cilia over time, it may be impractical to trigger cilia beats over a large area, and it is hypothesised that cilia lashes in a metachronal rhythm rather than in a coordinated fashion. In any event, the cilia's arrangement can be manipulated by the metachronal pattern outside of them. Respiratory path and reproductive system are carpeted with ciliated epithelium, which are the part of human body for fluid flow which express this movement. In the respiratory tract, cilia are found in the trachea, which aid in the inhalation of oxygen and the removal of dust and other hazardous particles to the outside. Various cilia may merge together to produce cirri in some animals. The cirri consists of tiny structures that serve as leg-like features. Lardner and Shack [1] claim that cilia rhythm is important in several physical processes in animals, including reproduction, rotation, breathing, alimentation, and locomotion. Ren et al. [3] devised an electrically controlled soft robotic polypyrrole bending actuators carpeted with cilia epidermis.

Nonetheless, metachronal rhythm may modify the curvature of cilia over their surface. It is quite worthy of discussion that metachronal rhythm develops the operative lash of the ciliary beat or the beating of the cilia is perpendicular to the direction of wave rhythm. There is some information available. In a conduit with two parallel oscillating walls, Akbar et al. [4] demonstrated physiological fluid flow rheology. Javed et al. [5] by relying on curvilinear system discussed the flow dynamics of aqueous electrolytic Newtonian fluid and provided a numerical model for the time-subordinate ciliary propulsion. Numerous biological fluids have non-Newtonian axioms, in view of the reported investigations [6–12]. Non-satisfactory consequences for the simple Newtonian fluid are investigated. The Power-Law Model is the most vibrantly used model for investigating rheological fluid transfer [13]. Because of its physiological nature, this power-law model relies on the fluid behaviour index n. This model gets close to both shear-thinning and shear thickening over a wide variety of rheological conditions. There are two methods for examining cilia motility irregularities: (i) The sublayer model (ii) The envelope model: it computes the forces along with twisting moments developed by each cilium toward adjoining fluid by obtaining the mean flow initiated by the ciliary layer. Hydrodynamic representation, on the other hand, is time-consuming and can be accomplished arithmetically. The envelope model has edge over other available models because it capitalizes on layer metachronal beats while ignoring sub-layer dynamic factors. Additionally, the envelope model is employed for quantitative investigations, such as velocities of swimming motion of microorganisms in water, which are measured quantitatively. Heat transfer analysis of ciliary driven nanofluids flow through ductus effrentes were comprehensively interrogated by Imran et al. [14, 15] and Bhatti et al. [16]. The heat phenomena along with mass transfer on dynamics of particle-fluid within an annulus were caused by cilia. The fluid transport characteristics in an inclined tube for a ciliary flow of fractional generalised Burgers and a Power law fluid model has been reported [17, 18] looked into it. Asghar et al. [19] focused on the mathematical analysis of a Newtonian system fluid transfer in a curved permeable channel due to ciliary metachronal waves. Saleem et al. [20] report on peristaltic flow as well as heat transfer of hybrid and phase ow for nano fluid models in a curved channel with ciliate tube. Elmaboud and Emam [21] investigated the effect of cilia in micropolar fluid transfer in a uniformly ciliated tube. Cilia oriented electro osmosis flow has been revealed by [22–26]. Researchers reported some useful result relating to EMHD flows [27–30]. Ramesd et al. [31] elaborated magnetohydrodynamic pumping of electro-conductive rheological fluid within ciliated micro-channel. The blood induced nanofluid transport through non-symmetric micro-channel with peristaltic phenomenon and revealed [32, 33] with the effects of radiation, buoyancy forces, and EMHD. Electrokinetics is chemical phenomenon in which relative dynamics of electrical field and a charged electric double layer is studied. Because of its enormous applications in bio-chemical engineering, mechanical miniaturization systems, electro-mechanical settings it has emerged as key research area nowadays [34–37]. Jang and Lee [38] pioneered the experimental investigation on electromagnetohydrodynamic (EMHD) for micro-pumps. The fluid transport in microchannel with EHMD was elaborated [39]. Jian and Chang [40] investigated numerical study for the EMHD flow along a slit microchannel. Inspired by contemporary novelty of joint investigations of electroosmosis, cilia wave and nanofluids, a mathematical model is proposed to reveal flow in microchannel governed by the mutual effects of cilia wave and electroosmosis. The crux of current investigation may be interpret as:

1. To model the cilia induce electro osmosis flow for nano fluids through tapered porous channel.
2. Non dimensionlize the governing equations and simplify them by utilizing low Reynolds number and long wavelength approximation.
3. Analytical solution intend to be extracted, wherever not possible numerical computations are employed.
4. Extensive graphical illustrations are presented to analyze the impact of various crucial emerging parameters.

Further the work is presented in systematic order as, Mathematical Interpretation of the Fluidic Problem, Dimensionless Analysis, Solution for the Novel Scheme, Graphical Analysis, and lastly Conclusion.

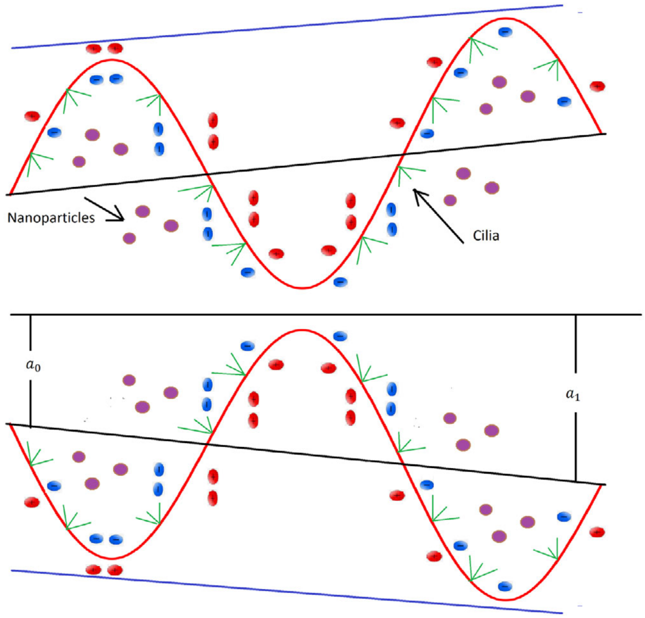

FIGURE 1 Geometry of cilia induce electro-osmotic flow through a tapered symmetric microchannel.

2 | MATHEMATICAL INTERPRETATION OF THE PHYSICAL PROBLEM

Let us evolve unsteady incompressible Newtonian nanofluid flow occupying in the permeable space in the symmetric tapered wavy ciliated channel. It is assumed that waves travels along the walls of the tapered ciliated symmetric micro-channel and this physiological phenomena is exhibited in Figure 1 and it can be presented as:

$$\widetilde{H}(\widetilde{X},t) = a + b\sin\left(\frac{2\pi}{\lambda}\right)(\widetilde{X} - ct), \tag{1}$$

in the above narrated equation $a = a_0 + k\widetilde{X}$ is the mean breadth of the tapered channel, a_0 is the width of the inlet and k is the non-uniform parameter, c is wave speed and λ is the wavelength.

The governing equations for fluid transport like continuity, momentum, energy, and relevant nanoparticle concentration can be provided as [24–26]:

$$\frac{\partial \widetilde{U}}{\partial \widetilde{\xi}} + \frac{\partial \widetilde{V}}{\partial \widetilde{\eta}} = 0, \tag{2}$$

$$\rho_f\left[\frac{\partial}{\partial t'} + \widetilde{U}\frac{\partial}{\partial \widetilde{\xi}} + \widetilde{V}\frac{\partial}{\partial \widetilde{\eta}}\right]\widetilde{U} = -\frac{\partial \widetilde{P}}{\partial \widetilde{\xi}} + \mu\left[\frac{\partial \widetilde{U}^2}{\partial \widetilde{\eta}^2} + \frac{\partial \widetilde{U}^2}{\partial \widetilde{\xi}^2}\right] - \frac{\mu}{k}\widetilde{U} + \rho_e E_x, \tag{3}$$

$$\rho_f\left[\frac{\partial}{\partial t'} + \left(\widetilde{U}\frac{\partial}{\partial \widetilde{\xi}} + \widetilde{V}\frac{\partial}{\partial \widetilde{\eta}}\right)\right]\widetilde{V} = -\frac{\partial \widetilde{P}}{\partial \widetilde{\eta}} + \mu\left[\frac{\partial^2}{\partial \widetilde{\xi}^2} + \frac{\partial^2}{\partial \widetilde{\eta}^2}\right]\widetilde{V} - \frac{\mu}{k}\widetilde{V}, \tag{4}$$

$$\begin{aligned}(\rho c')_f\left[\frac{\partial}{\partial t'} + \left(\widetilde{U}\frac{\partial}{\partial \widetilde{\xi}} + \widetilde{V}\frac{\partial}{\partial \widetilde{\eta}}\right)\right]\widetilde{T} = \widetilde{\kappa}\left[\frac{\partial^2}{\partial \widetilde{\xi}^2} + \frac{\partial^2}{\partial \widetilde{\eta}^2}\right]\widetilde{T} - \frac{\partial \widetilde{q}_r}{\partial \widetilde{\eta}} + \mu\left[4\left(\frac{\partial \widetilde{U}}{\partial \widetilde{\xi}}\right)^2 + \left(\frac{\partial \widetilde{V}}{\partial \widetilde{\xi}} + \frac{\partial \widetilde{U}}{\partial \widetilde{\eta}}\right)^2\right] \\ + (\rho c')_p\left[D_B\left(\frac{\partial \widetilde{C}}{\partial \widetilde{\xi}}\frac{\partial}{\partial \widetilde{\xi}} + \frac{\partial \widetilde{C}}{\partial \widetilde{\eta}}\frac{\partial}{\partial \widetilde{\eta}}\right)\widetilde{T} + \frac{D_T}{T_m}\left[\left(\frac{\partial \widetilde{T}}{\partial \widetilde{\xi}} + \left(\frac{\partial \widetilde{T}}{\partial \widetilde{\eta}}\right)^2\right)^2\right]\right],\end{aligned} \tag{5}$$

$$\left[\frac{\partial}{\partial t'} + \left(\widetilde{U}\frac{\partial}{\partial \widetilde{\xi}} + \widetilde{V}\frac{\partial}{\partial \widetilde{\eta}}\right)\right]\widetilde{C} = D_B\left[\frac{\partial^2 \widetilde{C}}{\partial \widetilde{\xi}^2} + \frac{\partial^2 \widetilde{C}}{\partial \widetilde{\eta}^2}\right] + \frac{D_T}{T_m}\left[\frac{\partial^2 \widetilde{T}}{\partial \widetilde{\xi}^2} + \frac{\partial^2 \widetilde{T}}{\partial \widetilde{\eta}^2}\right], \tag{6}$$

$\widetilde{U}, \widetilde{V}$ representing components of velocity along $\widetilde{\xi}$ and $\widetilde{\eta}$ axes, t', c' showing time, volumetric expansion coefficient, $\widetilde{P}$ signifying pressure σ' nanoliquid's electrical conductivity, ρ_f, ρ_p signifyng density for nanoliquid and nanoparticles respectively, $\widetilde{\kappa}$ thermal conductivity, Q_0 heat generation/absorption, D_B, D_T, T_m, and τ Brownian diffusion coefficient, thermophoretic diffusion coefficient, mean temperature of the nanoliquid and ratio of the effective heat capacity of nanoparticles substance and heat capacity of the nanoliquid respectively. The Poisson is introduced as

$$\rho_e = -\epsilon \nabla^2 \widetilde{\phi}. \tag{7}$$

3 | DIMENSIONLESS ANALYSIS

Introducing a wave frame (ξ, η) believe to have wave velocity c and is situated at some distance from stationary frame $\left(\widetilde{\xi}, \widetilde{\eta}\right)$, the reliable forth coming transformations may be utilised:

$$\xi + ct' = \widetilde{\xi}, \quad \eta = \widetilde{\eta}, \quad U + c = \widetilde{U}, \quad V = \widetilde{V}, \quad P = \widetilde{P}, \quad C = \widetilde{C}, \quad T = \widetilde{T}. \tag{8}$$

U, V representing velocity components in axial and transverse directions respectively, P is pressures, T is the temperature, and C nanoparticle volume fractions in the wave frame of references, respectively. Additionally to non dimensionalize the system of equations, it is worth to rely on the following non-dimensional quantities in Equations (1)–(6):

$$x = \frac{\widetilde{\xi}}{\lambda}, \quad y = \frac{\widetilde{\eta}}{a}, \quad \delta = \frac{d}{\lambda}, \quad t = \frac{ct'}{\lambda}, \quad u = \frac{\widetilde{U}}{c}, \quad v = \frac{\widetilde{V}}{c},$$

$$p = \frac{d^2 \widetilde{P}}{c\lambda\mu}, \quad Re = \frac{\rho_f ca}{\mu}, \quad \sigma = \frac{\widetilde{C} - C_0}{\overline{C}_1 - \overline{C}_0}, \quad \Pr = \frac{\mu c_f}{\widetilde{\kappa}}, \quad \theta = \frac{\widetilde{T} - T_0}{T_1 - T_0},$$

$$N_t = \frac{\tau D_T (T_1 - T_0)}{\upsilon T_m}, \quad N_b = \frac{\tau D_B (C_1 - C_0)}{\upsilon}, \quad \beta = \frac{Q_0 a^2}{(T_1 - T_0)\upsilon c_p}, \quad R_n = \frac{16\overline{\sigma} T_0^3}{3\overline{\kappa}\mu c_f}, \quad \phi = \frac{\widetilde{\phi}}{\zeta}.$$

Invoking Debye–Hückel linearization, the reputed Poisson-Boltzmann Equation may take simplified form as:

$$\frac{\partial^2 \phi}{\partial y^2} = m^2 \phi, \tag{9}$$

Moreover, utilising the low Reynolds number and long wave length simplifications, the governing Equations become

$$\frac{\partial p}{\partial x} = \frac{\partial^2 u}{\partial y^2} - \frac{1}{k} u + \beta\, m^2 \phi, \tag{10}$$

$$\frac{\partial p}{\partial y} = 0, \tag{11}$$

$$(1 + \Pr R_n) \frac{\partial^2 \theta}{\partial y^2} + (B_r) \left(\frac{\partial u}{\partial y} \right)^2 + (\Pr N_b) \left(\frac{\partial \sigma}{\partial y} \frac{\partial \theta}{\partial y} \right) + (\Pr N_t) \left(\frac{\partial \theta}{\partial y} \right)^2 = 0, \tag{12}$$

$$\frac{\partial^2 \sigma}{\partial y^2} + \frac{N_t}{N_b} \frac{\partial^2 \theta}{\partial y^2} = 0. \tag{13}$$

Equation (13) forecast that $p \neq p(y)$, so

$$\frac{dp}{dx} = \frac{\partial^2 u}{\partial y^2} - \frac{1}{k} u + \beta\, m^2 \phi, \tag{14}$$

$u = -1 - 2\pi\epsilon\alpha\delta\, Cos\, 2\pi x, \Phi = 1, \theta = 1, \sigma = 1$, at

$$y = h = 1 + m_1 x + \alpha \sin 2\pi x, \tag{15}$$

$\frac{\partial u}{\partial y} = 0, \sigma = 0, \theta = 0, \Phi = 0$ at

$$y = 0, \tag{16}$$

4 | SOLUTION FOR THE NOVEL SCHEME

Extracting the exact analytical solution for the Equation (9) as

$$\phi(y) = \frac{(e^{2my} - 1)e^{hm-my}}{e^{2hm} - 1}. \tag{17}$$

Exact Expression for the axial velocity may gathered as

$$u(y) = \frac{1}{(e^{2hm} - 1)(km^2 + 1)} e^{-my} \sec\left(\frac{h}{\sqrt{k}}\right)\Bigg(2\beta k^{3/2} m^3 e^{m(h+y)} \sin\left(\frac{h-y}{\sqrt{k}}\right)$$
$$- (e^{2hm} - 1)e^{my} \cos\left(\frac{y}{\sqrt{k}}\right)\left(k^2 m^2 \frac{dp}{dx} + k\left(m^2(\beta - \mathrm{u0}) + \frac{dp}{dx}\right) - \mathrm{u0}\right) - k\cos\left(\frac{h}{\sqrt{k}}\right)$$
$$\left(-\frac{dp}{dx}(km^2+1)e^{m(2h+y)} + \beta m^2 e^{hm} - \beta m^2 e^{m(h+2y)} + \frac{dp}{dx}(km^2+1)e^{my}\right)\Bigg). \tag{18}$$

The expression for volume flux is obtained as

$$Q = \frac{1}{(-1+e^{2hm})(1+km^2)}\sqrt{k}\Bigg(\sqrt{k}\left((-1+e^{2hm})h(1+km^2)\frac{dp}{dx} - m(-1-e^{2hm}+2e^{hm}(1+km^2))\beta\right)$$
$$+ 2e^{hm}k^{3/2}m^3\beta \mathrm{Sec}\left[\frac{h}{\sqrt{k}}\right] - (-1+e^{2hm})\left(k^2m^2\frac{dp}{dx} - \mathrm{u0} + k\left(\frac{dp}{dx} + m^2(-\mathrm{u0}+\beta)\right)\right)\mathrm{Tan}\left[\frac{h}{\sqrt{k}}\right]\Bigg). \tag{19}$$

Expression stream function may be obtained using the relation $u = \frac{\partial\psi}{\partial y}$

$$\psi(y) = -\left(\frac{y\left(\sqrt{k}\left(-2\beta k^{3/2}m^3e^{hm} - (e^{2hm}-1)\sin\left(\frac{h}{\sqrt{k}}\right)(-k\beta m^2 + km^2\mathrm{u0} + \mathrm{u0})\right) + \right.}{k(e^{2hm}-1)(km^2+1)\left(\sqrt{k}\sin\left(\frac{h}{\sqrt{k}}\right) - h\cos\left(\frac{h}{\sqrt{k}}\right)\right)}\right.$$
$$\left.\frac{\left.\cos\left(\frac{h}{\sqrt{k}}\right)(\beta km(2e^{hm}(km^2+1) - e^{2hm} - 1) + Q(e^{2hm}-1)(km^2+1))\right)}{k(e^{2hm}-1)(km^2+1)\left(\sqrt{k}\sin\left(\frac{h}{\sqrt{k}}\right) - h\cos\left(\frac{h}{\sqrt{k}}\right)\right)}\right), \tag{20}$$

Expression for the pressure gradient is obtained from solving Equation (19) for $\dfrac{dp}{dx}$,

$$\frac{dp}{dx} = \frac{1}{(e^{2hm}-1)(km^2+1)\left(hk - k^{3/2}\tan\left(\frac{h}{\sqrt{k}}\right)\right)}\Bigg(\beta k^{3/2}m^2e^{2hm}\tan\left(\frac{h}{\sqrt{k}}\right) - \beta k^{3/2}m^2\tan\left(\frac{h}{\sqrt{k}}\right)$$
$$+ k^{3/2}m^2\mathrm{u0}(-e^{2hm})\tan\left(\frac{h}{\sqrt{k}}\right) + k^{3/2}m^2\mathrm{u0}\tan\left(\frac{h}{\sqrt{k}}\right) + 2\beta k^2m^3e^{hm} - 2\beta k^2m^3e^{hm}\sec\left(\frac{h}{\sqrt{k}}\right) + km^2Qe^{2hm}$$
$$+ 2\beta kme^{hm} - \beta kme^{2hm} - \sqrt{k}\mathrm{u0}e^{2hm}\tan\left(\frac{h}{\sqrt{k}}\right) + \sqrt{k}\mathrm{u0}\tan\left(\frac{h}{\sqrt{k}}\right) + Qe^{2hm} - km^2Q - \beta km - Q\Bigg). \tag{21}$$

If we put $\alpha = 0, \beta = 0, \delta = 0$ in Equation (10) and Equation (15) the result of ref. [26] are recovered.

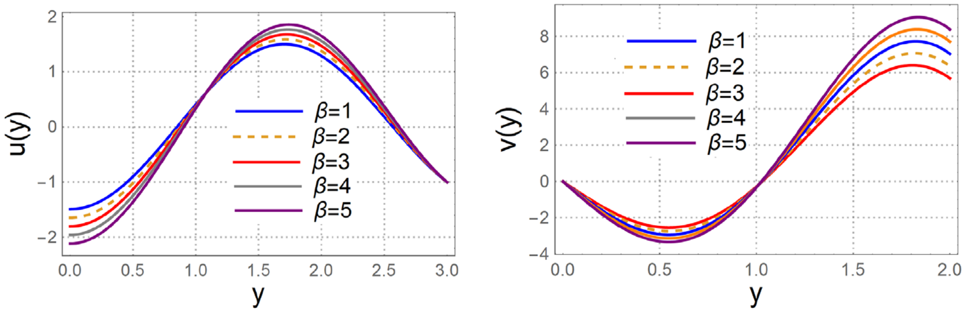

(a) (b)

FIGURE 2 Investigation of β on velocity profile with $\alpha = 0.2, \epsilon = 0.12, Q = 0.6, x = 1, \delta = 0.01, k = 0.29, m = 0.7$.

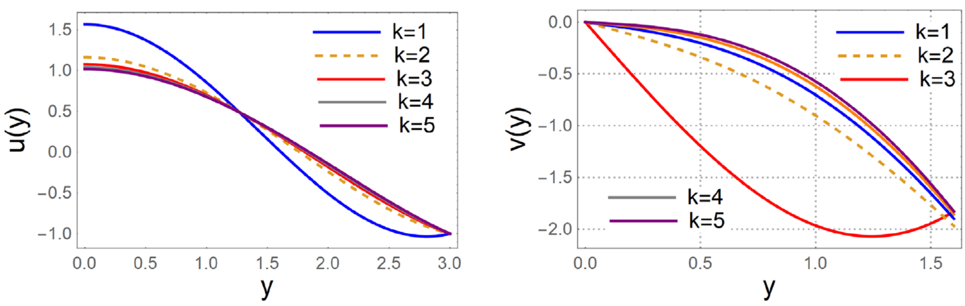

(a) (b)

FIGURE 3 Investigation of k on velocity profile with $\alpha = 0.2, \epsilon = 0.12, Q = 0.6, \delta = 0.01, \beta = 2, m = 0.7$.

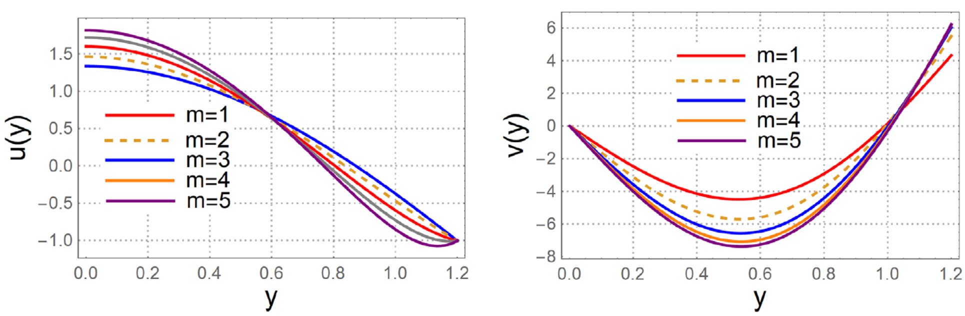

(a) (b)

FIGURE 4 Investigation of m on velocity profile with $\alpha = 0.8, \epsilon = 0.12, Q = 0.6, \delta = 0.01, k = 2, \beta = 2$.

5 | GRAPHICAL ANALYSIS

In this investigation, a comprehensive study has been made to reveal electro osmosis flow through a tapered ciliated porous channel. It is assumed the flow is initiated because of metachronal dynamics of cilia. Axial electric field is deployed and thermal radiation phenomenon is scrutinized by applying convective conditions. In this juncture of investigation variation of pertinent crucial parameters on the velocity profile, temperature and concentration profiles, pressure gradient, pressure rise per wavelength, and on the velocity distribution inside the micro ciliated is presented. In Figures 2–4 impact of Helmholtz—Smoluchowski velocity β, permeability parameter k, and electro osmotic parameter m on the axial and transverse segment of velocity are exhibited. Figure 2 reveal that as the value of β is strengthened both axial and transverse components of velocity show deterioration in regions $y \ni [0, 1]$ and then surge in the velocity profiles is observed in $y\epsilon[1, 3]$. It is worth to know that the electric field presence with ions near the vicinity of the double layer, retard nanofluid flow and initiate a productive slip velocity in exterior regime of double layer, is known as Helmholtz–Smoluchowski

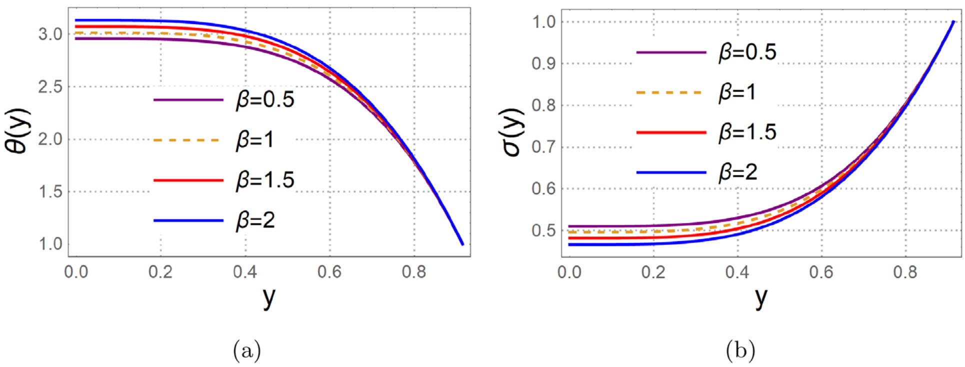

FIGURE 5 Plots of nanoparticle temperature and concentration as function of β with $\alpha = 0.3, \epsilon = 0.12, m = 1.5,$ $\delta = 0.01, p_r = 0.5, N_t = 0.1, k = 1.5, Q = 0.6, x = 0.9, R_n = 0.1.$

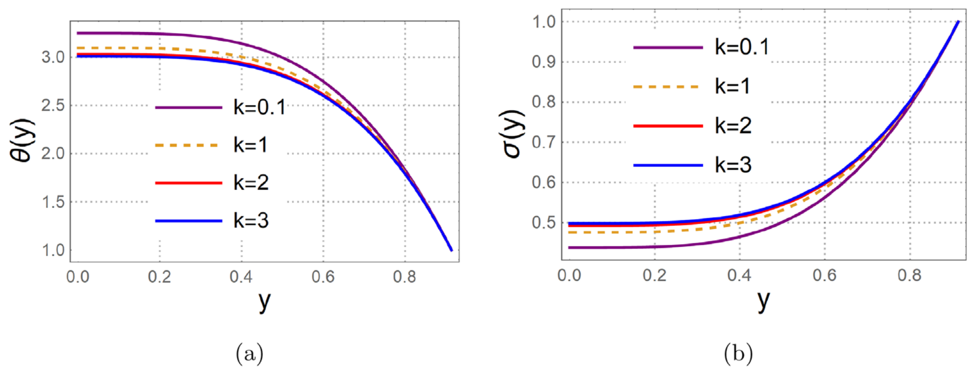

FIGURE 6 Variation of k nanoparticle temperature and concentration with $\alpha = 0.3, \epsilon = 0.12, m = 1.5, m_1 = 0.1$ $\delta = 0.01, p_r = 0.5, N_t = 0.1, \beta = 1.5, Q = 0.6, x = 0.9, R_n = 0.1.$

velocity. Effect of permeability parameter k is interrogated in Figure 3. Axial velocity is initially suppressed near flow regime $y\epsilon[0, 1.5]$ and then rise in the fluid is seen in the region $y\epsilon[1.2, 3]$, whereas, mere surge in transverse velocity is evident. The behaviour of electro osmotic parameter on flow dynamic in the ciliated tapered microchannel is exhibited in Figure 4. Electroosmotic transport is initiated by Coulomb force which is induced due to electric field for net mobile electric charge. Due to prevalence of chemical equilibrium of a solid surface with an electrolyte solution results in interface hiring of net electrical charge, and electrical double layer or Debye layer develops in the vicinity interface. Axial velocity due to increase in m is elevated at the start of the flow and in the middle of flow regime quite opposite scenario is observed, on other hand transverse velocity is quit appreciably reduced. The nanoparticles temperature along with concentration profiles are examined for different value of Helmholtz–Smoluchowski velocity β, permeability parameter k, electro osmotic parameter m, radiation parameter Rn, and Brinkman number Br in Figures 5–9. Figure 5 exhibit that nanoparticle temperature is lowered as value of β is strengthened, in contrary nanoparticle concentration become vigorous. One can easily noticed from Figure 6, with the rise in the permeability phenomenon there is rise in the temperature of the nanofluid, which mean in this case suction effect is dominating, on other hand diffusion phenomena of the nanofluid is affected with enhancing permeability. It is concluded from Figure 7 that electro osmotic parameter m slow down the heat transfer phenomenon and on other hand it give rise to nano particles concentration profile. Impact of thermal radiation parameter on the nanoparticle temperature and concentration profiles is revealed in the Figure 8. Rise in temperature profile is evident from with enhancement in thermal radiation phenomenon, which is quite natural observation. Additionally, contrast behaviour in nanoparticle concentration is recorded. It signifies that the external radiation escalate the temperature, and simultaneously movement of the particle is diluted. This phenomenon may prove great significance in the biological fluid dynamic in the field of medical science. In Figure 9, Impact of Brinkman number Br on nanoparticle temperature and concentration is exhibited. The temperature of the nano fluid particles is enhanced with the augmented value of of Brinkman number. It is quite established fact in a scenario when the temperature is enhanced, the gap around the molecules enhances due to decline in cohesiveness. Which result decrease in the viscosity of nanofluids

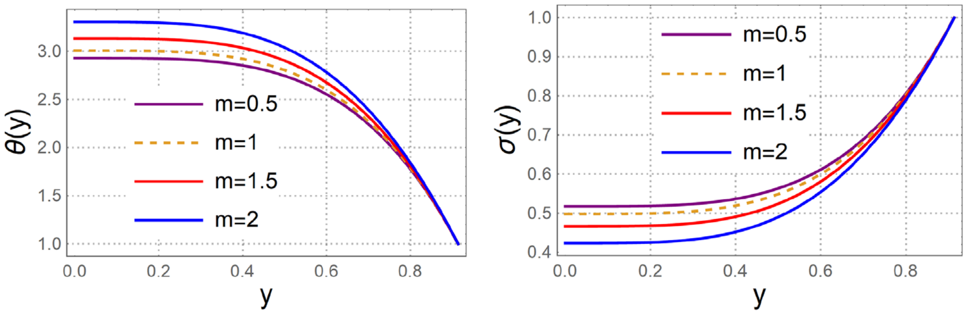

(a) (b)

FIGURE 7 Variation of m nanoparticle temperature and concentration with $\alpha = 0.3, \epsilon = 0.12, k = 1.2, \delta = 0.01, p_r = 0.5, N_t = 0.1, \beta = 2, Q = 0.6, k = 1, m_1 = 0.1, x = 0.9, R_n = 0.1$.

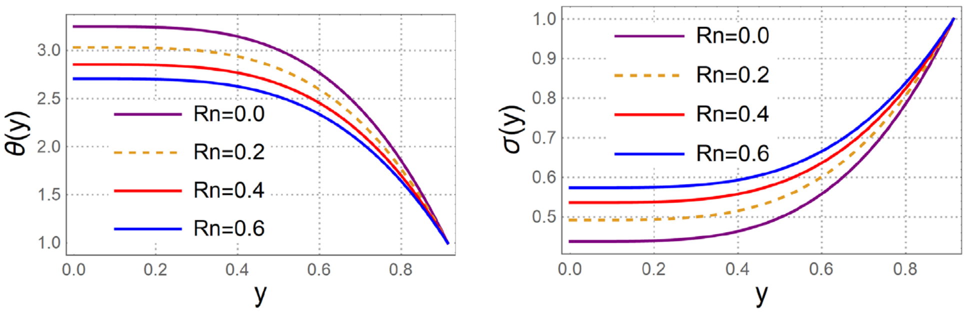

(a) (b)

FIGURE 8 Impact of thermal Radion nanoparticle temperature and concentration with $\alpha = 0.3, \epsilon = 0.12, k = 1.2, \delta = 0.01, p_r = 0.5, N_t = 0.1, \beta = 2, Q = 0.6, x = 0.9, R_n = 0.1$.

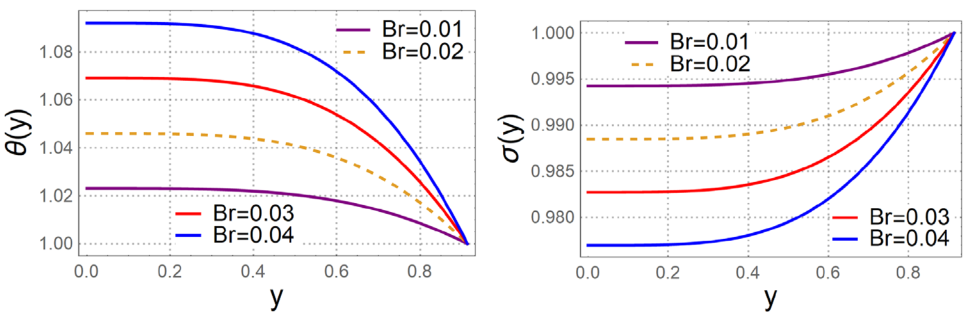

(a) (b)

FIGURE 9 Analysis of Br on nanoparticle temperature and concentration with $\alpha = 0.3, \epsilon = 0.12, k = 1.2, \delta = 0.01, p_r = 0.5, N_t = 0.1, \beta = 2, Q = 0.6, x = 0.9, R_n = 0.1, m_1 = 0.1$.

happened when the nanoparticle temperature is raised. Pumping mechanism for the flow inside the non uniform ciliated micro channel is investigated in Figure 10. It has been revealed that pressure gradient profile is suppressed for enhancing value of β and k, its means these parameters ultimately play a role in slowing down the transport phenomenon inside the channel. Figure 11 illustrate that effect of α and m on the pumping mechanism. It has been observed that pumping phenomena is dominating in $x\epsilon[0, 0.5]$ flow regime and weak in $x\epsilon[0.5, 1]$. On other hand appreciable rise in the pressure gradient profile is reported for electro osmotic parameter m. Figure 12 demonstrate that pressure rise per wave length profile is also declined for augmented values of β and k. Trapping phenomenon which has pivotal role in the physiological processes is explored in Figures 13–14. It is reported that size of the trapped bolus is magnified with escalation in Helmholtz–Smoluchowski velocity β. Further more it is quite evident from Figure 14 that size of the trap bolus is squeezed

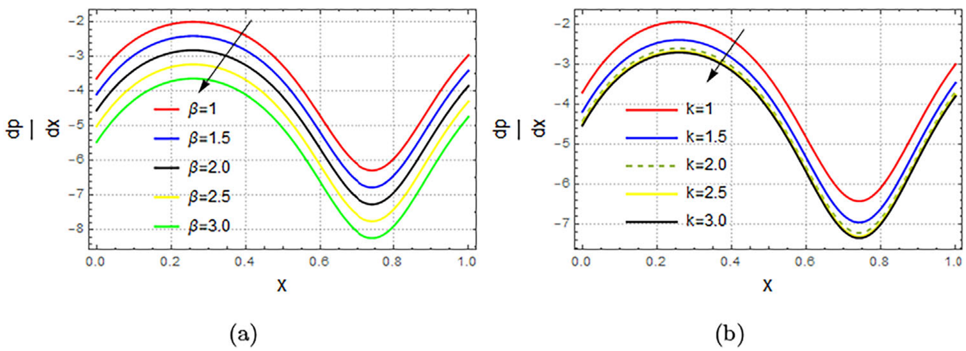

FIGURE 10 Analysis of β and k on pressure gradient along with $\alpha = 0.3, \epsilon = 0.12, \delta = 0.01, m_1 = 0.1,$ $(a)\, k = 1,$ $(b)\, \beta = 1.$

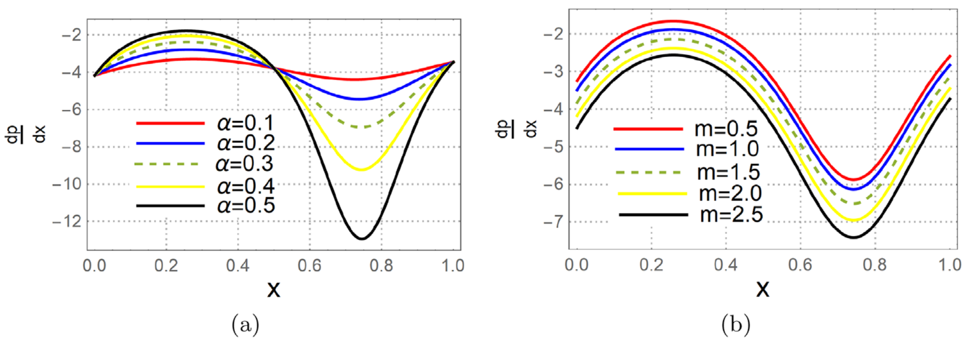

FIGURE 11 Analysis of α and m on pressure gradient along with $\beta = 1, k = 1$ $\epsilon = 0.12, \delta = 0.01, m_1 = 0.1,$ $(a)\, m = 1,$ $(b)\, \alpha = 0.3.$

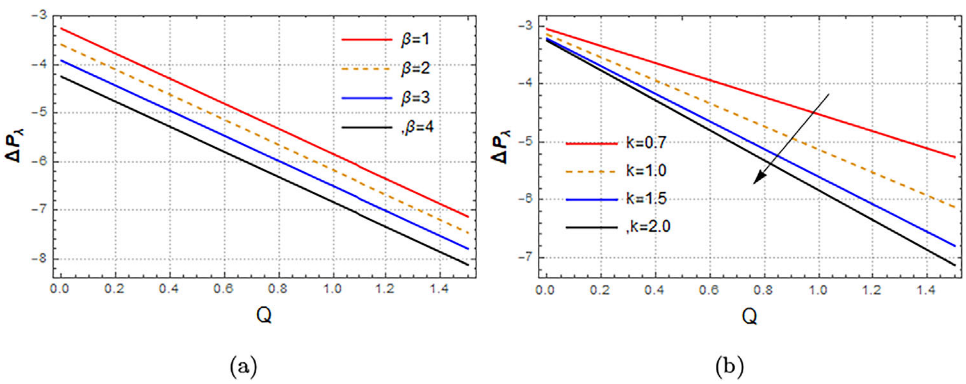

FIGURE 12 Analysis of β and Permeability parameter k on pressure rise profile with $\alpha = 0.3, \epsilon = 0.12,$ $\delta = 0.01, m_1 = 0.1,$ $(a)\, k = 2,$ $(b)\, \beta = 1.$

with increasing permeability. Variations of heat transfer coefficient is extensively elaborated in Figure 15. It is reported that heat transfer coefficient is enhanced with Prandtl number and declined with radiations parameter (see Figure 15a). Whereas the heat transfer coefficient remain invariant for m, k, and β.

6 | CONCLUSION

A broad study has been made to reveal electro osmosis flow through a tapered ciliated symmetric porous channel. It was assumed that flow initiated due to metachronal dynamics of cilia and axial electric field is taken along thermal radiation phenomenon and convective boundary conditions. The pertinent equations of motion were non dimensionalized and simplified by capitalizing the low Reynolds number and long wave length approximations. Exact novel analytical solution

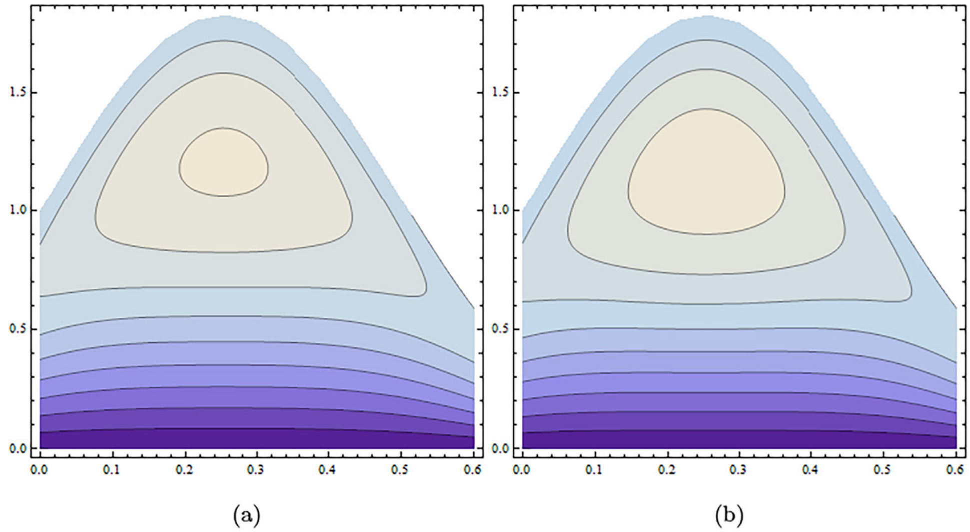

FIGURE 13 Analysis of β on the velocity distribution profile with $\alpha = 0.8, \epsilon = 0.12,$ $\delta = 0.01, m = 0.8, m_1 = 0.1, k = 2,$ $(a)\ \beta = 1,$ $(b)\ \beta = 2.$

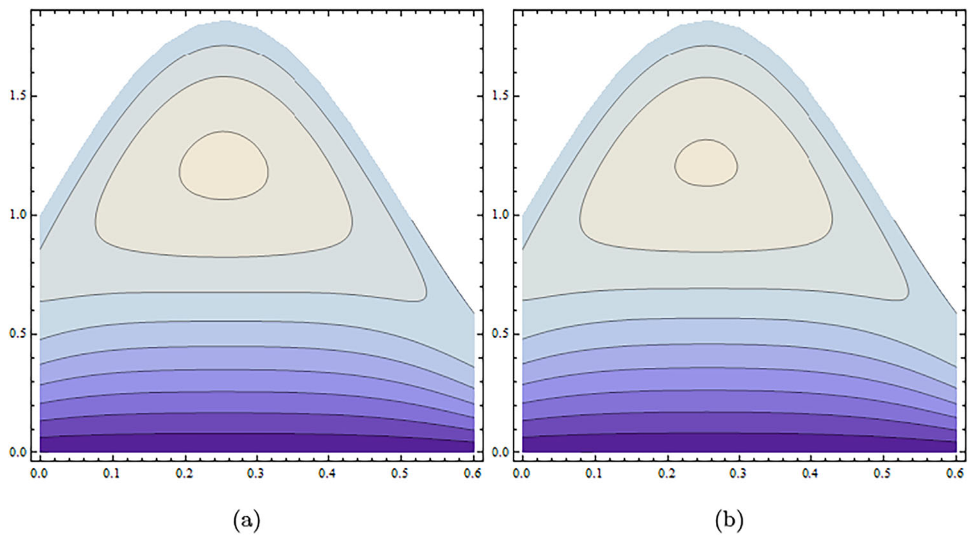

FIGURE 14 Streamlines variation as function of k $\alpha = 0.8, \epsilon = 0.12, Q = 0.6, \delta = 0.01, m = 1.5, \beta = 1,$ $(a)\ k = 2,$ $(b)\ k = 3.$

is gathered for Poisson equation and the axial velocity. Additionally, traverse velocity, temperature and nanofluids concentration profiles are scrutinized via numerical computations. The main outcomes of current investigation may be culminated as:

1. Axial velocity is declined with Helmholtz–Smoluchowski velocity β and permeability parameter k, whereas transverse velocity shows the same behaviour for β, but for k it only shows increase in the velocity profile.
2. Temperature profile is declined β, k, and electro osmotic parameter m, but the concentration profile is declined with β and is elevated for k and m.
3. Temperature profile is improved for the increasing values of thermal radiation and for Brinkman number and reverse behaviour is seen for nano particle concentration profile.
4. Pumping phenomenon is retarded as Smoluchowski velocity and permeability are strengthened.
5. Smoluchowski velocity and permeability play a predominant role in trapping mechanism.

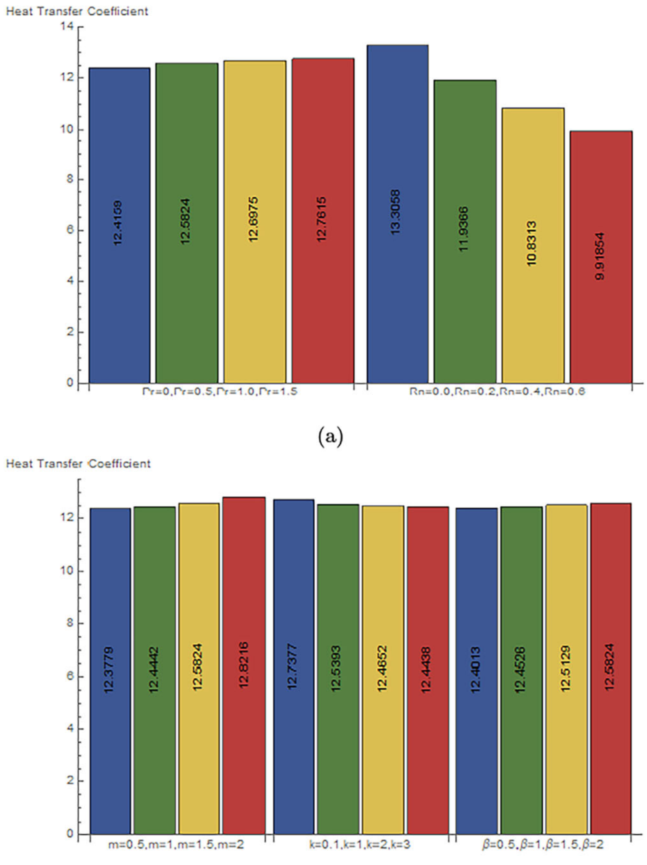

(a)

(b)

FIGURE 15 Analysis of heat transfer coefficient along with $\beta = 1, k = 1\ \epsilon = 0.12, \delta = 0.01, m_1 = 0.1, m = 1, \alpha = 0.3$.

In future electro osmosis flow through a tapered ciliated symmetric porous channel may be considered for non-Newtonian fluid by adding further physical effects double diffusive convection and implementing slip at the wall. Moreover for further analysis one may investigate stochastic numerical computing based solver [41–44] for the investigation of Electro Osmotic Flow of Nanofluids [45].

ACKNOWLEDGEMENTS

The authors have nothing to report.

ORCID

Ali Imran https://orcid.org/0000-0002-4349-1570
Saeed Ehsan Awan https://orcid.org/0000-0002-4557-9533
Muhammad Asif Zahoor Raja https://orcid.org/0000-0001-9953-822X

REFERENCES

[1] Lardner, T.J., Shack, W.J.: Cilia transport. Bull. Math. Biol. 34, 325–335 (1972)
[2] Rivera, J.A.: Cilia, Ciliated Epithelium, and Ciliary Activity. Pergamon Press, New York (1962)
[3] Ren, Z., Zhang, M., Song, S., Liu, Z., Hong, C., Wang, T., Dong, X., Hu, W., Sitti, M.: Soft-robotic ciliated epidermis for reconfigurable coordinated fluid manipulation. Sci. Adv. 8(34), eabq2345 (2022)
[4] Akbar, N.S., Tripathi, D., khan, Z.H., Anwar Bég, O.: Mathematical modelling of pressure-driven micropolar biological flow due to metachronal wave propulsion of beating cilia. Math. Biosci. 301, 121–128 (2018)
[5] Javid, K., Riaz, M., Chu, Y.M., Khan, M.I., Khan, S.U., Kadry, S.: Peristaltic activity for electro-kinetic complex driven cilia transportation through a non-uniform channel. Comput. Methods Programs Biomed. 200, 105926 (2021)
[6] Khedher, N.B., Ijaz, N., Zeeshan, A., Saleem, N., Ali, S.S., Zouidi, F., Riaz, A., Tag-ElDin, E.M.: Measurement of thermal radiative and mass transfer of peristaltic pumping of electrically-conducting bio-bi-phase flow due to metachronal wave: Eukaryotic cells in biological applications. Case Stud. Therm. Eng. 49, 103196 (2023)

[7] Aich, W., Javid, K., Al-Khaled, K., Gachem, K., Khan, D., Khan, S.U., Kolsi, L.: The ciliated flow of water-based graphene oxide and copper nanoparticles (GO-Cu/H2O) in a complex permeable tube with entropy generation phenomenon. Waves Random Complex Media (2022). https://doi.org/10.1080/17455030.2022.2056261

[8] Joshua, K., Golla, V.K.A.: Magnetic peristaltic ciliary flow regulates an embryo growth in the human fallopian tube. Biointerface Res. Appl. Chem. 13(1), 55 (2023)

[9] Akram, J., Akbar, N.S.: Electroosmotically actuated peristaltic-ciliary flow of propylene glycol + water conveying titania nanoparticles. Sci. Rep. 13(1), 11801 (2023)

[10] Alharbi, K.A.M., Riaz, A., Sikandar, S.: An entropy model for Carreau nanofluid ciliary flow with electroosmosis and thermal radiations: A numerical study. Electrophoresis 45(13–14), 1112–1129 (2023).

[11] Karmakar, P., Barman, A., Das, S.: EDL transport of blood-infusing tetra-hybrid nano-additives through a cilia-layered endoscopic arterial path. Mater. Today Commun. 36, 106772 (2023)

[12] Maiti, S., Pandey, S.K.: Rheological fluid motion in tube by metachronal waves of cilia. Adv. Appl. Math. Mech. 38(3), 393–410 (2017)

[13] Imran, A., Akhtar, R., Zhiyu1, Z., Shoaib, M., Raja, M.A.Z.: Heat transfer analysis of biological nanofluid flow through ductus efferentes. AIP Adv. 10, 035029 (2020). https://doi.org/10.1063/1.5135298

[14] Imran, A., Akhtar, R., Zhiyu, Z., Shoaib, M., Raja, M.A.Z.: Analysis of MHD and heat transfer effects with variable viscosity through ductus efferentes. AIP Adv. 9(8), 085320 (2019). https://doi.org/10.1063/1.5110433

[15] Bhatti, M.M., Elelamy, A.F., Sait, S.M., Ellahi, R.: Hydrodynamics interactions of metachronal waves on particulate-liquid motion through a ciliated annulus: application of bio-engineering in blood clotting and endoscopy. Symmetry 12(4), 532 (2020)

[16] Maqbool, K., Mann, A.B., Siddiqui, A.M., Shaheen, S.: Fractional generalized Burgers' fluid flow due to metachronal waves of cilia in an inclined tube. Adv. Mech. Eng. 9(8), 1687814017715565 (2017)

[17] Siddiqui, A.M., Sohail, A., Maqbool, K.: Analysis of a channel and tube flow induced by cilia. Appl. Math. Comput. 309, 133–141 (2017)

[18] Asghar, Z., Javid, K., Waqas, M., Ghaffari, A., Khan, W.A.: Cilia-driven fluid flow in a curved channel: effects of complex wave and porous medium. Fluid Dyn. Res. 52(1), 015514 (2020)

[19] Saleem, A., Akhtar, S., Alharbi, F.M., Nadeem, S., Ghalambaz, M., Issakhov, A.: Physical aspects of peristaltic flow of hybrid nano fluid inside a curved tube having ciliated wall. Results Phys. 19, 103431 (2020)

[20] Elmaboud, Y.A., Emam, T.G.: Cilia transport for micropolar fluid through a uniform cylindrical tube. Appl. Appl. Math. 13(1) (2018)

[21] Khan, W.U., Imran, A., Raja, M.A.Z., Shoaib, M., Awan, S.E., Kausar, K., He, Y.: A novel mathematical modeling with solution for movement of fluid through ciliary caused metachronal waves in a channel. Sci. Rep. 11(1), 20601 (2021)

[22] Imran, A., Waheed, A., Javeed, S., Baleanu, D., Zeb, M., Ahmad, S.: Investigation of electroosmosis flow of copper nanoparticles with heat transfer due to metachronal rhythm. Therm. Sci. 25(Spec. issue 2), 193–198 (2021)

[23] Alfwzan, W.F., Imran, A., Allehiany, F.M., Aldhabani, M.S.: A mathematical model for cilia actuated transport of Gold–Silver hybrid nanofluid EMHD flow with activation energy phenomena. Case Stud. Therm. Eng. 103252 (2023)

[24] Imran, A., Raja, M.A.Z., Shoaib, M., Zeb, M., Nisar, K.S.: Electro-osmotic transport of a Williamson fluid within a ciliated microchannel with heat transfer analysis. Case Stud. Therm. Eng. 45, 102904 (2023)

[25] Alhazmi, S.E., Imran, A., Awais, M. et al.: Thermal convection in nanofluids for peristaltic flow in a nonuniform channel. Sci. Rep. 12, 12656 (2022). https://doi.org/10.1038/s41598-022-16600-w

[26] Prakash, J., Tripathi, D., Tiwari, A.K., Sait, S.M., Ellahi, R.: Peristaltic pumping of nanofluids through a tapered in a porous environment: applications in blood flow. Symmetry 11(7), 868 (2019)

[27] Abbasi, A., Al-Khaled, K., Zouidi, F., Khan, S.U., Khan, M.I., Bafakeeh, O.T., Farooq, W., Choudhari, R.: Blood-based electro-osmotic flow of non-Newtonian nanofluid (Carreau-Yasuda) in a tapered channel with entropy generation. Z. Angew. Math. Mech. 103(5), e202100351 (2023)

[28] Li, D., Li, K.: Time periodic pulse electroosmotic flow of Jeffreys fluids through a parallel plate microchannel. Z. Angew. Math. Mech. 102(4), e202000391 (2022)

[29] Khan, Z.H., Akbar, N.S., Akram, J., Hamid, M., Wei, Y.: Electroosmotically augmented peristaltic flow of carbon nanotubes based nanofluid through asymmetrical channel. Z. Angew. Math. Mech. e202100354 (2023)

[30] Wu, M., Yang, J., Zhang, X., Yang, W., Yu, J.: Neural network-based adaptive region tracking control for robot manipulator systems with uncertain kinematics and dynamics. Z. Angew. Math. Mech. e202300383 (2023)

[31] Ramesh, K., Tripathi, D., Bég, O.A.: Cilia-assisted hydromagnetic pumping of biorheological couple stress fluids. Propul. Power Res. 8(3), 221–233 (2019)

[32] Vemulawada, S., Jayavel, P., Verma, A., Ghachem, K., Kolsi, L., Ramesh, K.: Thermal analysis on electromagnetic regulated peristaltic blood-based graphane/diamond nanofluid flow with entropy optimization. Numer. Heat Transfer, Part B Fundamentals 84(5), 514–538 (2023)

[33] Ramesh, K., Tripathi, D., Bhatti, M.M., Ghachem, K., Khan, S.U., Kolsi, L.: Mathematical modeling and simulation of electro-magnetohydrodynamic bio-nanomaterial flow through physiological vessels. J. Appl. Biomater. Funct. Mater. 20, 22808000221114708 (2022)

[34] Tripathi, D., Prakash, J., Gnaneswara Reddy, M., Kumar, R.: Numerical study of electroosmosis-induced alterations in peristaltic pumping of couple stress hybrid nanofluids through microchannel. Indian J. Phys. 95(11), 2411–2421 (2021)

[35] Akram, J., Akbar, N.S., Tripathi, D.: Analysis of electroosmotic flow of silver-water nanofluid regulated by peristalsis using two different approaches for nanofluid. J. Comput. Sci. 62, 101696 (2022)

[36] Imran, A., Raja, M.A.Z., Awan, S.E., Shoaib, M.: Analysis of radiative heat transfer on electro-osmotic magneto nanofluid flow through ciliary propulsion. Z. Angew. Math. Mech. e202300689 (2024). https://doi.org/10.1002/zamm.202300689
[37] Allehiany, F.M., Alqudah, M., Imran, A., Alqarni, M.M., Mahmoud, E.E.: A novel computational investigation for EMHD gold nanofluids in an asymmetric inclined ciliated microchannel. Ain Shams Eng. J. 102611 (2024)
[38] Jang, J., Lee, S.S.: Theoretical and experimental study of MHD (magnetohydrodynamic) micropump. Sens. Actuators A 80(1), 84–89 (2000)
[39] Chakraborty, S., Paul, D.: Microchannel flow control through a combined electromagnetohydrodynamic transport. J. Phys. D: Appl. Phys. 39(24), 5364 (2006)
[40] Jian, Y., Li, F., Liu, Y., Chang, L., Liu, Q., Yang, L.: Electrokinetic energy conversion efficiency of viscoelastic fluids in a polyelectrolyte-grafted nanochannel. Colloids Surf. B 156, 405–413 (2017)
[41] Awan, S.E., Ali, F., Awais, M., Shoaib, M., Raja, M.A.Z.: Intelligent Bayesian regularization-based solution predictive procedure for hybrid nanoparticles of AA7072-AA7075 oxide movement across a porous medium. Z. Angew. Math. Mech. 103(10), e202300043 (2023)
[42] Wahid, M.A., Bukhari, S.H.R., Maqsood, M., Aadil, F., Khan, M.I., Awan, S.E.: Parametric estimation scheme for aircraft fuel consumption using machine learning. Neural Comput. Appl. 35(35), 24925–24946 (2023)
[43] Awan, S.E., Awais, M., Shamim, R., Raja, M.A.Z.: Novel design of intelligent Bayesian networks to study the impact of magnetic field and Joule heating in hybrid nanomaterial flow with applications in medications for blood circulation. Tribol. Int. 189, 108914 (2023)
[44] Khan, S., Awan, S.E., Muhammad, Y., Jadoon, I., Raja, M.A.Z.: Novel polynomial Abet data augmentation algorithm with GRU paradigm for nuclear power prediction. Ann. Nucl. Energy 201, 110441 (2024)
[45] Abbasi, A., Al-Khaled, K., Zouidi, F., Khan, S.U., Khan, M.I., Bafakeeh, O.T., Farooq, W, Choudhari, R.: Blood-based electro-osmotic flow of non-Newtonian nanofluid (Carreau-Yasuda) in a tapered channel with entropy generation. Z. Angew. Math. Mech. 103(5), e202100351 (2023)

How to cite this article: Imran, A., Abbas, M., Awan, S.E., Shoaib, M., Raja, M.A.Z.: Electro osmotic flow of nanofluids within a porous symmetric tapered ciliated channel. Z Angew Math Mech. e202300838 (2024). https://doi.org/10.1002/zamm.202300838